ORNL/TM-2003/107

Metals and Ceramics Division

Correlation of Process Data and Electrochemical Noise to Assess Kraft Digester Corrosion: Spring Grove Experiment

S. J. Pawel*
D. W. Townley†
D. E. Roy‡
D. F. Wilson*

*Metals and Ceramics Division, ORNL, Oak Ridge, TN
†M. J. Schiff and Associates, Claremont, CA
‡Glatfelter Company, Spring Grove, PA

Date Published: April 2003

Prepared for
U. S. Department of Energy
Office of Industrial Technologies

Prepared by the
OAK RIDGE NATIONAL LABORATORY
Oak Ridge, TN 37831-6285
Operated by
UT-Battelle, LLC
for the
U. S. DEPARMENT OF ENERGY
Under contract DE-AC05-00OR22725

This page
intentionally blank

PREFACE

Dimensions and calculated quantities using these dimensions are given in English units rather than in the unified metric system throughout this report. Fundamentally, the vessel dimensions (feet and inches), the measurement locations associated with the digester (feet and inches), wall thickness measurements (inches and mils), and corrosion rates (mils/y) provided by the mill are recorded and discussed in English units. As a result, and because it is the common nomenclature for mill personnel and the anticipated audience of this document, these units will be retained for use in the report. Conversion to metric system units depends on the following relationships:

1 mil = 0.001 in. = 0.0254 mm
1 inch = 25.4 mm
1 foot = 0.305 m

This page
intentionally blank

CONTENTS

Page

This page
intentionally blank

TABLES

This page
intentionally blank

FIGURES

This page
intentionally blank

ACRONYMS AND SYMBOLS

ECN	Electrochemical Noise
EX	extraction screens
ID	inside diameter
LI	localization index
ORNL	Oak Ridge National Laboratory
ZRA	zero resistance ammeter
Ag/Ag_2S	silver/silver sulfide reference electrode
e+	unit charge of electricity
I	current
m	charge on metallic ion produced by corrosion process
M	atomic weight of corroding material
N_o	Avagadro's number (6.023 x 10-19/mol)
P	penetration
Q	integrated current sum over exposure time t
R_n	resistance noise parameter
t	exposure time
W	mass dissolving as a result of corrosion in time t

This page
intentionally blank

ABSTRACT

Electrochemical noise (ECN) probes were deployed in a carbon steel continuous kraft digester at four locations and at one location in the bottom cone of the associated flash tank. The probes consisted of carbon steel electrodes, representing the vessel construction material, and 309LSi stainless steel overlay electrodes, representing the weld overlay repair in a portion of the vessel. Current and potential noise, the temperature at each probe location, and the value of about 32 process parameters (flow rates, liquor chemistry, etc.) were monitored continuously for a period of almost one year. Historical vessel inspection data and post-test evaluation of the probe components were used to assess/compare ECN corrosion activity with physical changes in wall thickness and corrosion patterns on the digester shell. In addition, attempts were made to correlate ECN activity from each electrode type with process parameters.

The results indicate the high general corrosion rates of steel observed just below the extraction screens – on the order of 35 mils/y for the past few years – accelerated further during the period of probe deployment. The maximum wastage of steel (normalized to one full year exposure) was about 85 mils/y at the ring 6N probe just below the extraction screens. Consistent with recent historical observations, the steel corrosion rate at the ring 6S probe – at the same elevation but directly across the digester from ring 6N – was significantly lower at about 50 mils/y. Just prior to probe deployment, the digester shell below the extraction screens was overlaid with 309LSi stainless steel, which was observed to be essentially immune to corrosion at this location. While the ECN probes detected differences in electrochemical behavior between steel probes and between 309LSi probes at rings 6N and 6S, there was only poor quantitative correlation of current sums with actual corrosion rates at these locations. A significant contribution of redox reactions on both steel and stainless steel electrodes appears to complicate ECN interpretation for all the probes, but particularly at the ring 6 locations.

With the exception of start-up and shutdown activity, including brief upsets for “hanging columns” or brief maintenance periods, no correlation was observed between tracked process variables and ECN activity. Based on the ECN data, re-pressurization of the digester and resumption of chip/liquor feed after a brief disruption results in very aggressive corrosion events.

This page
intentionally blank

1.0 INTRODUCTION

This is the second in a series of reports detailing experiments involving deployment of electrochemical noise (ECN) corrosion probes in an operating digester. The initial report [1] includes introductory remarks about digesters and assessments of corrosion problems during operation. In summary of that information, the ECN technique has a number of potential advantages over more traditional/standard techniques to assess digester corrosion, including:

- ECN affords real time measurement of corrosion activity (compared to roughly annual assessments of cumulative damage on witness coupons);
- ECN does not apply a displacement potential (which avoids disruption of corrosion films or processes);
- ECN can differentiate general and localized corrosion (where other real-time techniques such as thin-layer activation are not able to assess pitting or cracking); and
- ECN captures the synergisms of the process (where lab studies outside the process are often chemically sterile – for example, organic components of the pulping process are often omitted – or omit flow and other process variables).

Of course, there are also limitations of the ECN technique. The most obvious are that it tends to be much more expensive than witness coupons and it requires more experience and data gathering equipment than many other techniques. Further, it is difficult to obtain precise/quantitative corrosion rate information from ECN probes. The reasons are many, but fundamentally, the ECN technique monitors net current flow between two nominally identical electrodes through a zero resistance ammeter (ZRA). Several factors influence the magnitude of current flowing through the ZRA, including the magnitude of wastage corrosion activity on each electrode in the measurement pair, how much corrosion current self-terminates (has anodes and cathodes on the same electrode rather than on opposite electrodes), and the relative magnitude of the redox activity. Therefore, at least until a calibration database for each particular process is built, the ECN technique more typically provides a real-time measurement of qualitative corrosion activity.

Unlike the digester examined in the initial experiment [1], the Spring Grove digester is an older vessel with a long history of relatively trouble-free service. It was put into service in 1965, but not until recently has the digester begun to experience high general corrosion rates

and, perhaps, limited pitting in specific portions of the vessel. Mill personnel were willing to add ports to the digester vessel to study corrosion and, based on results from recent inspections indicating points of potential interest, ECN probes were positioned at four locations in the digester. In addition, a corrosion probe was installed in the bottom cone of a liquor flash tank.

Like the previous report [1], the purpose of this document is to report data gathered from a group of ECN probes deployed in an operating continuous digester and to attempt to correlate the corrosion activity detected by the probes with corresponding operating parameters and historic inspection data to assess corrosion in the vessel.

2.0 SPRING GROVE DIGESTER

2.1 GENERAL DESCRIPTION

The digester fitted with ECN probes in this experiment is located in Spring Grove, PA at the Glatfelter Company pulp mill. The digester is a carbon steel Kamyr vessel commissioned in 1965. The vessel has pulped exclusively pine species – mostly southern pine – using conventional continuous cooking and, until recently, has experienced relatively little corrosion/wastage problems. However, coincident with a number of changes over the last few years (discussed in subsequent sections), general corrosion has increased dramatically in the lower portions of the vessel such that the minimum allowable wall thickness was being approached in some locations.

A schematic diagram of the Spring Grove digester appears in Fig. 1. The vessel is approximately 150 ft. tall and 12 ft. in diameter, and the relative positions of the ECN probes for this experiment are indicated on the schematic drawing. The number associated with each probe was determined from the ring section number of the shell it represents and, in the case of the two probes at a single elevation, the further notation “N” and “S” describes the relative side of the vessel. The “N” designation indicates the probe on the northeast side of the vessel with approximately the same longitude as the service manway. The “S” designation indicates the probe in the southwest portion of the vessel almost directly across the vessel from the probe at the “6N” location. The probes at ring 3 and ring 12 have the same vessel longitude, which is only very slightly different from the longitudinal position of the probe at ring 6N. More information on the probes is given in a subsequent section.

In addition to the four probes indicated in Fig. 1, a fifth probe was located in the bottom cone of the #1 liquor flash tank. The flash tank is carbon steel construction and has experienced corrosion rates sufficient to warrant replacement of the internal dished head in the late 1990s. The flash tank probe was identical in design and detail to the other probes, but due to data gathering limitations, was only used during the final three months of the initial experiment.

Table 1 gives the probe locations along with approximate corresponding elevations as well as the original shell thickness at that location. Generally, the original shell thickness values are

not recorded measurements but the minimum thickness requirement for the steel used to fabricate the vessel. In many cases, the actual original thickness was not recorded except that it met or exceeded the required value. As a rule of thumb, the original thickness requirement at each location in the digester includes 0.250 in. for corrosion allowance.

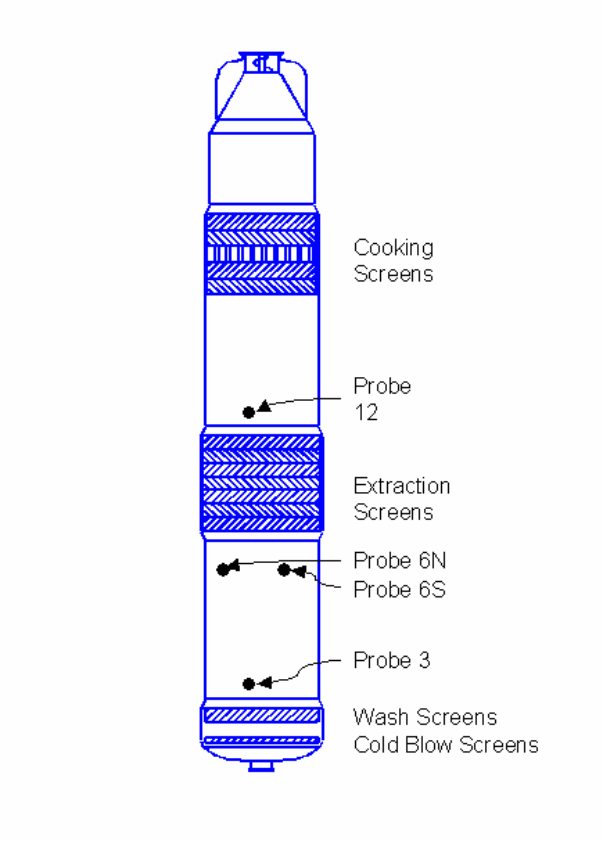

Fig. 1. Schematic of the Spring Grove digester and probe locations.

Table 1. Position/location of electrochemical noise probes in the Spring Grove digester.

Probe ID	Location/Elevation relative to other components	Design Shell Thickness (in.)
Ring 3	≈ 8 ft. above top of wash screens, just above manway	1.332
Ring 6N	≈ 6 ft. below bottom row of extraction screens, above manway	1.289
Ring 6S	≈ 6 ft. below bottom row of extraction screens, opposite 6N	1.289
Ring 12	≈ 8 ft. above top row of extraction screens	1.438
Flash Tank	≈ mid-slope in bottom cone of vessel #1	0.375

2.2 ULTRASONIC THICKNESS DATA

Routine ultrasonic thickness measurements have been collected for the digester shell since at least the late 1970s, although some of the documentation was not available to ORNL. Wall thickness data have been collected at about 60 external locations – fixed and labeled positions under the vessel insulation – on an approximately annual basis. Wall thickness data at internal locations have also been routinely collected at four equi-spaced locations at each of two elevations in each ring section of the digester. While all of the data exhibit significant scatter, the external data appear to offer the most promise for consistent interpretation because the measurement locations do not change from year to year and there is little variation in surface condition (roughening due to corrosion or the presence of adherent corrosion products) at the external measurement locations.

Figure 2 shows the wall thickness as a function of time measured externally at two specific points on the digester. The location indicating the greatest extent of thinning is on ring section 6 just below the extraction (EX) screens, where the corrosion rate has been historically higher than other locations in the vessel. The other location is just above the EX screens (ring section 12), where corrosion has been historically much more modest than below the EX screens.

Figure 2 is representative of several important features in the wall thickness data. Fundamentally, it indicates that the wall thickness measurements are somewhat erratic. For example, the significant wall thickness increase indicated from 1978 to 1979 (observed for all of the data collected in 1979 – not just the two locations discussed here) is certainly not real and likely indicates a systematic measurement/calibration error. [Data for 1979 was not used in the placement of the trend line.] Smaller wall thickness increases were also periodically observed indicating the sensitivity of the measurement technique to practical factors such as surface conditions, skill of the craftsman, and calibration details. It also shows the importance of using data that span several years to determine an overall trend rather than relying on data from consecutive years to judge the condition of the vessel or the current rate of thinning.

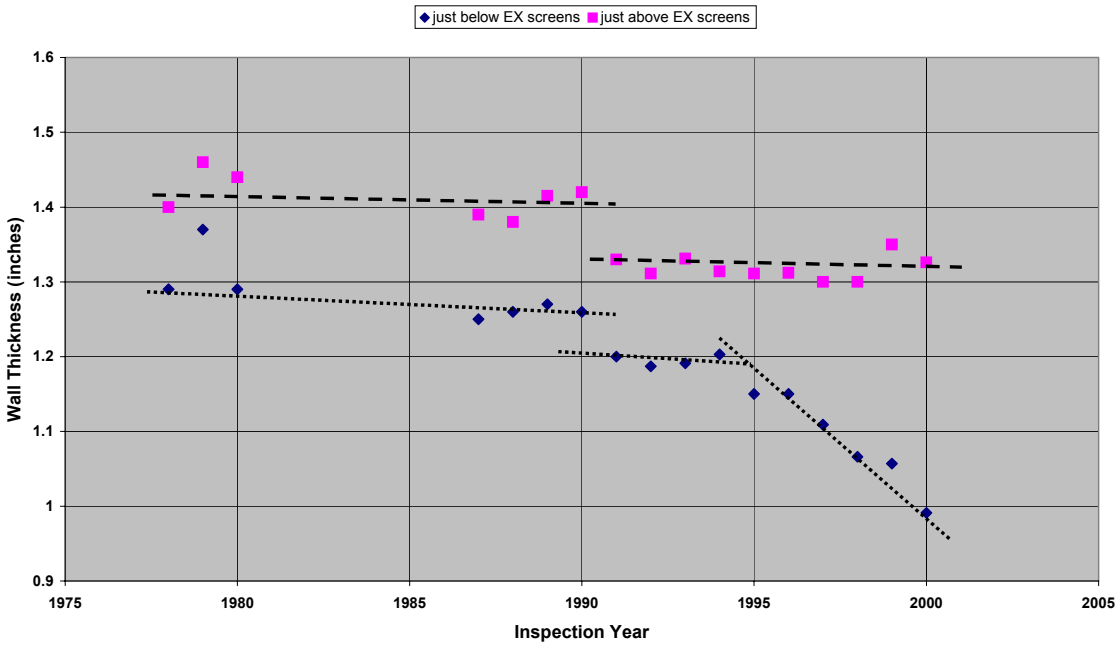

Fig. 2. Wall thickness as a function of time for a position on ring 6 (just below the extraction screens) and ring 12 (just above the extraction screens).

Further, the data in Fig. 2 show that the general thinning of the vessel – as indicated by the slope of the approximate trend curves – remains relatively constant through the 1980s into the early 1990s, although there appears to be a step-function change in the thickness recorded at these (and most other) points in the vessel between 1990 and 1991. It is suspected that a change in measurement technique and equipment was employed beginning in 1991, but there is insufficient documentation to confirm the hypothesis. Based on the slope of the trend curves for thickness as a function of time, the digester shell just above the EX screens (ring 12) has been thinning at a rate of approximately 1-2 mils/y for approximately 20 years. Just below the EX screens (ring 6), the rate of thinning through the 1980s and early 1990s was only slightly greater – perhaps 3-4 mils/y – until a dramatic change occurred sometime around the 1994 inspection. From 1994 through 2000, the rate of thinning appears to average approximately 35-40 mils/yr at this location.

Lower in the vessel, the ultrasonic thickness data also indicates an increased rate of thinning in the last few years, but it is not as dramatic as the accelerated corrosion just below

the EX screens (and perhaps begins at a different time). Based on the data shown in Fig. 3, the general thinning rate over the last few years appears to be about 15-20 mils/y at ring 3.

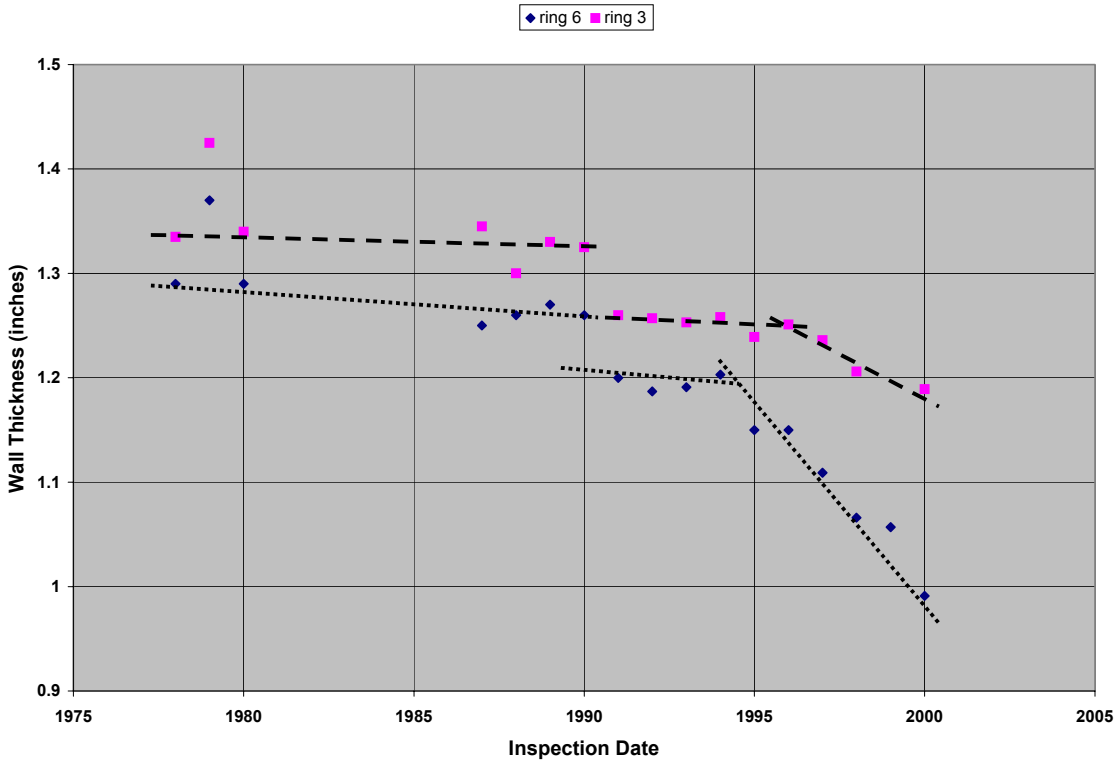

Fig. 3. Wall thickness as a function of time for a position on ring 6 (just below the extraction screens) and on ring 3 (just above the wash screens).

Due in part to the apparent accelerated corrosion on rings 5 and 6, these two shell sections immediately below the EX screens were overlaid with 309LSi stainless steel during the June 2000 maintenance outage. The overlay – which covered the entire circumference over a vertical height of about 20 ft. – was applied with automatic welding machines to a nominal thickness of 3/16 in. Just prior to the overlay application, a series of ultrasonic thickness measurements was performed in an array of 10 locations per elevation (evenly spaced around the diameter) at six elevations (four ft. intervals) over the area to be overlaid.

The result of this assessment indicated that wastage of the vessel was not uniform on these sections of the digester. A representative survey for an elevation just beneath the EX screens (top portion of ring 6, similar to the elevation of the point below the EX screens in Fig. 2) is shown in Fig. 4. The thickness variation among the ten measurement locations at this elevation is significant, and the difference between the maximum (point 6) and minimum (point 1) thickness is 88 mils. The average difference between maximum and minimum thickness for the six different elevations in the measurement array was 82 mils, with the minimums (point 1 or 2) and maximums (points 6, 7, or 8) always occurring at the same general longitude.

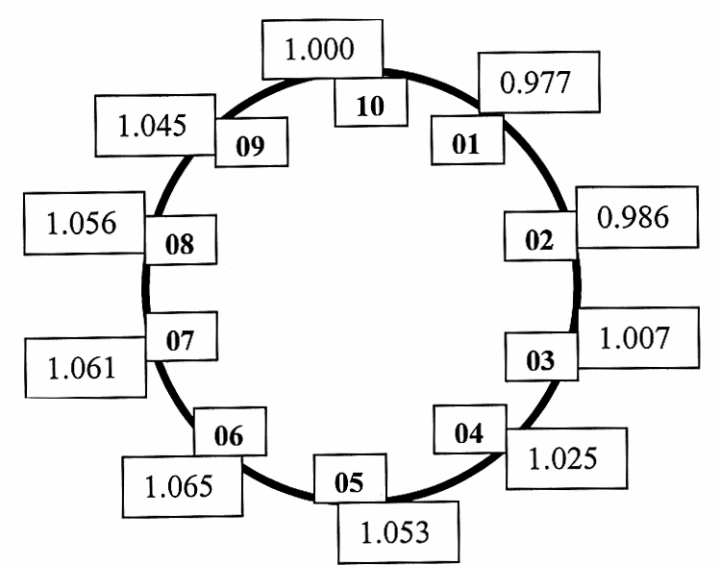

Fig. 4. Schematic diagram representing the wall thickness measurement pattern at a series of elevations on rings 5 and 6. The numbers inside the circle represent the fixed measurement location numbers, and the values associated with each outside the circle are the specific wall thickness values (in.) collected near the top of ring 6.

As a result of this thickness pattern, two ECN probes were located at the same elevation in ring 6 – one in the northeast portion (position 1 in Fig. 4), representing the high wastage rate, and one in the southwest region (position 6 in Fig. 4), representing the lowest wastage rate at the elevation. The overlay activity was complete prior to cutting the holes for the ECN probes.

When the plug pieces from the hole-cutting were examined, it was confirmed that the shell in the southwest portion of ring 6 was almost 100 mils thicker than the equivalent location on the opposite side of the digester.

2.3 Visual Inspection Prior to Probe Deployment

During the June 2001 maintenance outage, the digester was available for internal inspection. To prepare for inspection, the vessel was acid cleaned with inhibited 2% formic acid at 52°C (125°F) for about 12 h followed by water rinsing. Despite the cleaning activity, residual black liquor remained on much of the vessel walls, which potentially obscured some details of surface condition of the vessel. Inspection observations are organized here from bottom to top of the vessel.

The digester shell between the cold blow screens and the wash screens exhibited a variety of colors ranging from black to red/orange resulting from residual black liquor and flash rusting, but only very minor surface relief and roughness – with no pitting – was observed. The visible portion of the wash screens appeared new and completely unattacked but, despite the recent acid cleaning, significant portions of the wash screens were clogged (Fig. 5) with a gray “crud” that was quite viscous and pasty. Mill personnel believed the material to be soap.

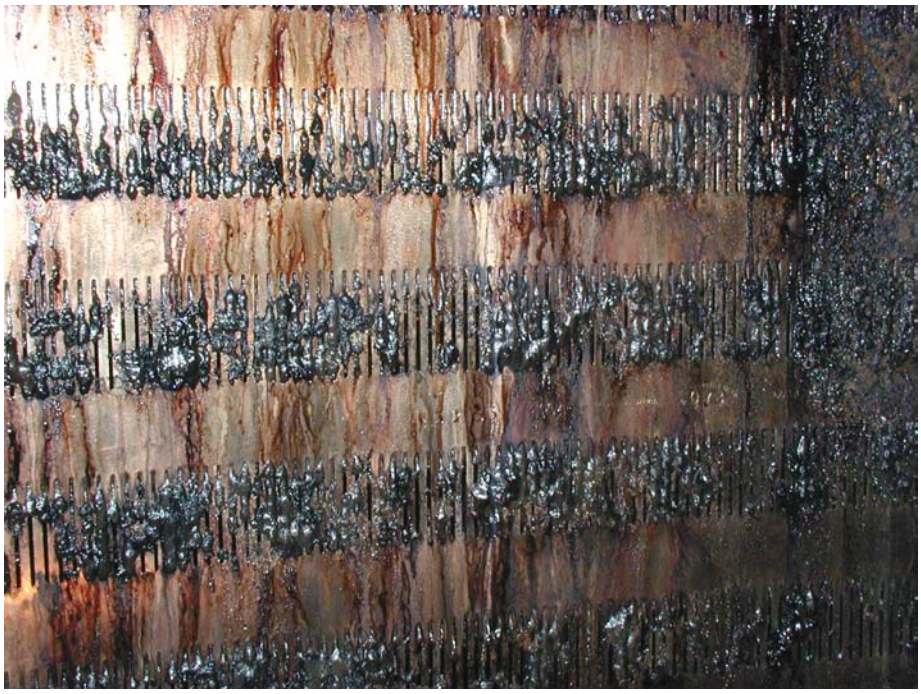

Fig. 5. Appearance of wash screens (ring 1). For scale, the vertical slots in the screens are about 6 inches long.

On the shell surfaces at the elevation of the service manway (ring 3) just above the wash screens, scattered light "pitting" was observed in some areas (Fig. 6). The bottom and sides of the roughly circular pits were smooth and well-rounded and, based on depth gage measurements, approximately 40-50 mils deep. As has been observed in some other digesters [1], the pits in this particular area were generally the same depth and the shell surfaces between pits were smooth and uniform. There is little support documentation, but anecdotal evidence suggests these pits first appeared several years ago and have not obviously spread or become significantly deeper since the initial observation. One of the ECN probes was located on ring 3 near the manway.

Fig. 6. Light pitting observed on the shell in ring 3 at the June 2001 inspection. At top, the general area around the port for the ring 3 probe is shown (with manway at far right). At bottom, a close-up view showing typical pits about 40-50 mils deep and 0.5 inch diameter. The bottom photograph was taken at high incidence angle to reveal pit depth.

Moving higher in the vessel, the shell surfaces on rings 4-7 (up to the bottom of the EX screens) appeared relatively smooth with no evidence of localized corrosion or erosion patterns. Despite the ultrasonic thickness data indicating a recently accelerated corrosion rate, particularly on the shell surfaces of rings 5-6, the walls at this location do not show signs of a high corrosion rate, such as irregular surface relief or non-uniform corrosion product accumulations. Rather, the shell was found to be very smooth to the touch and free of surface relief except for the slightly raised seam welds (see Fig. 7). It is possible that the acid cleaning procedure acts to remove corrosion products and, along with the erosion of the process itself, smooth the vessel surfaces, thus disguising the amount/intensity of corrosion at this location.

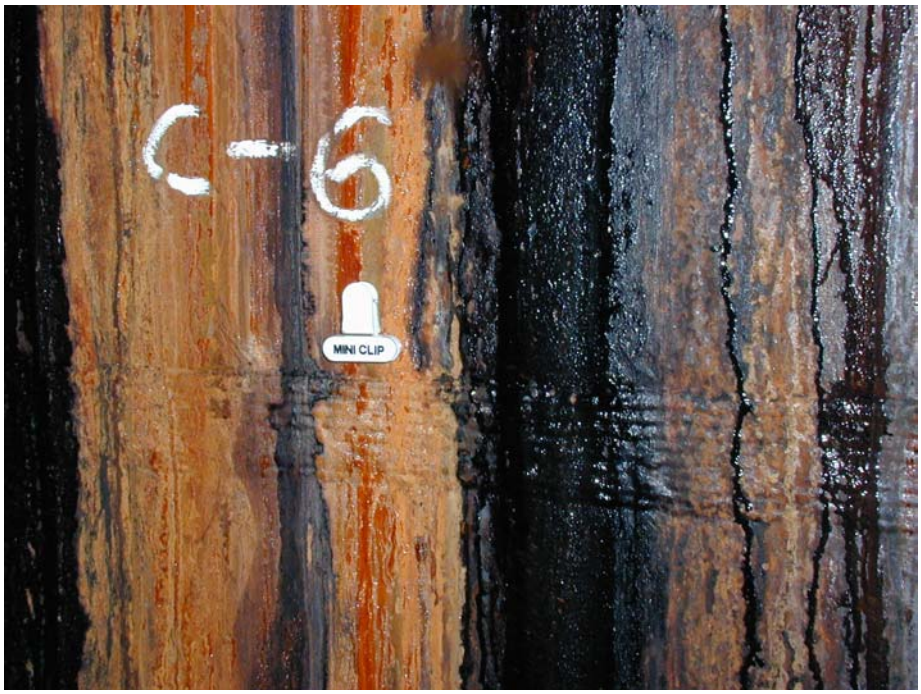

Fig. 7. Circumferential weld C6 at the June 2001 inspection. The weld joins ring sections 5 and 6 and is approximately 12 ft. below the bottom extraction screen. At this location, the weld bead crown retains some solidification detail and protrudes slightly above the shell ID. In other positions around the circumference, this weld appears to have suffered general wastage such that it no longer protrudes above the shell ID. The 1.5 in. wide mini-clip is present to indicate relative magnification.

In the absence of additional wall thickness data, the only apparent sign of degradation in this portion of the digester was recession of portions of the weld at C-6 (round seam weld between rings 5 and 6). Mill personnel indicated that the entire round seam weld at this location was repaired in June 2000 to build-up the weld crown such that it stood above the shell ID by about 1/16 in. However, only one year later (at the time of the present inspection), this round seam weld had suffered wastage such that the weld surface was again recessed below the shell ID by about 1/16 in. over approximately half of the circumference. Curiously, the side of the digester suffering the most significant weld wastage is not the same side of the vessel that has suffered the highest average rate of shell thinning over the past few years. This observation suggests the area/side of the vessel subject to the most intense corrosion may move periodically as a function of an unidentified variable associated with irregular flow or process chemistry. Alternatively, the composition/structure of the weld may be sufficiently different from the shell material that different factors influence corrosion.

The extraction screen surfaces were smooth and unattacked but a thick and viscous paste waste clogged most of the EX screen surface (Fig. 8). Mill personnel collected a specimen of this material for analysis, and identified the material as fatty acids, esters, organic pitch, and soap.

Fig. 8. View of extraction screens showing extensive clogging.

The shell between the EX screens and the cooking screens (rings 12-14) exhibited a relatively uniform light pitting, which had not been observed previously. In most areas, the pit depth was approximately 20-25 mils (Fig. 9), although it was possible to find isolated pits that were somewhat deeper. While not a precise trend, the area fraction of the pitting seemed to increase without a corresponding increase in pit depth as elevation in the digester increased from ring 12 to ring 15 (compare Fig. 9 with Fig. 10). The circumferential seam welds in this region did not stand above the shell ID, indicating at least some amount of wastage has occurred since the most recent repair date (approximately 1995). The center pipe at this elevation of the digester also showed scattered light pitting (Fig. 11).

Fig. 9. Circumferential weld C12 at the June 2001 inspection. The weld joins ring sections 11 and 12 just above the extraction screens. The weld is uniformly corroded such that the surface is recessed slightly compared to the shell ID. Light pitting (20-25 mils deep) is generally present on the shell surfaces at this location. The scale marker (mini-clip) is 1.5 in. wide.

Fig. 10. Appearance of shell wall on ring 13 at the June 2001 inspection. The unpitted area (raised, slightly shiny in the photograph) has agglomerated such that it is a small fraction of the total area at this elevation. However, based on the height of the "islands," the depth of pitting has not increased and remains 20-25 mils. Scale marker (mini-clip) is 1.5 in. wide.

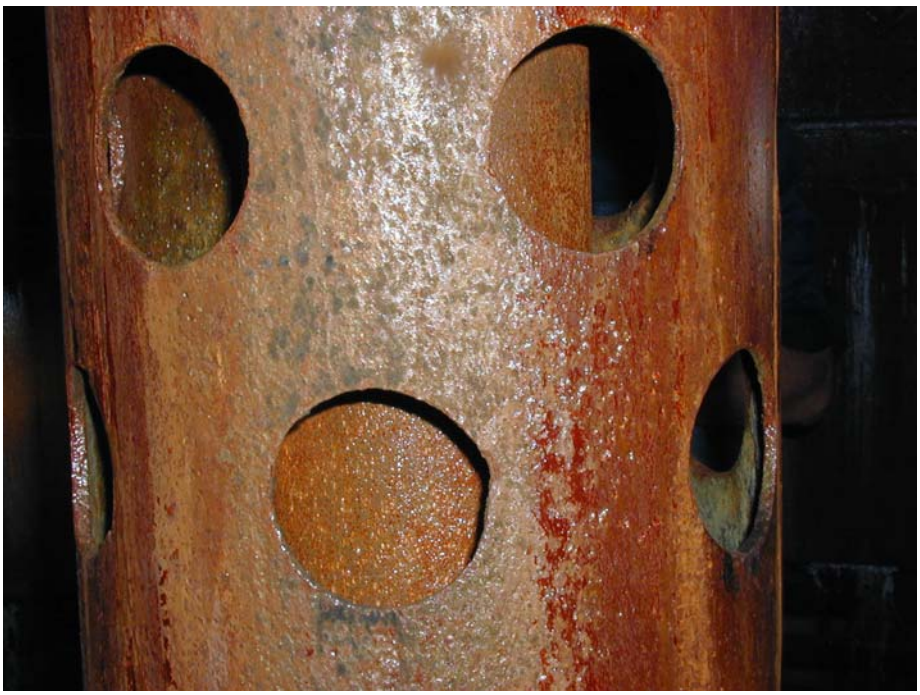

Fig. 11. Appearance of the center pipe at the elevation of ring 12 (just above the extraction screens). Light pitting similar to that observed in the digester shell at this elevation is apparent.

The cooking screens and blank plates appeared largely smooth and unattacked, as were the shell surfaces above the cooking screens. On the transition piece from the shell to the top cone, there were a few gouges on the order of 60-70 mils deep. Based on size and location, these appear to be associated with positions at which grinding was once required to remove a fixture. Figure 12 is representative of this observation.

Fig. 12. Near the top of the vessel (C20), deep gouges were observed with a size/shape and location indicative of the position of fixtures associated with construction. From the June 2001 inspection.

Following the visual inspection, the automated welding equipment was installed and the overlay activity on rings 5 and 6 commenced. The overlay material was type 309LSi stainless steel, applied automatically in overlapping vertical beads about 3/4 in. wide and 3/16 in. thick. Figure 13 shows the top edge of the weld overlay and the track for the automated welding equipment. The overlay applied in June 2001 covered the entire diameter from just below the

extraction screens to an elevation approximately 20 feet lower in the vessel. Figure 14 shows the region where the upper and lower overlay applications in June 2001 overlapped, and Fig. 15 presents one of the (few) minor repairs required after the overlay was completed but before the vessel was restarted.

Fig. 13. Automated welding equipment and the top edge of the weld overlay area inside the digester. June 2001 overlay application.

Fig. 14. View of region where upper and lower overlay zones overlap. June 2001 overlay application.

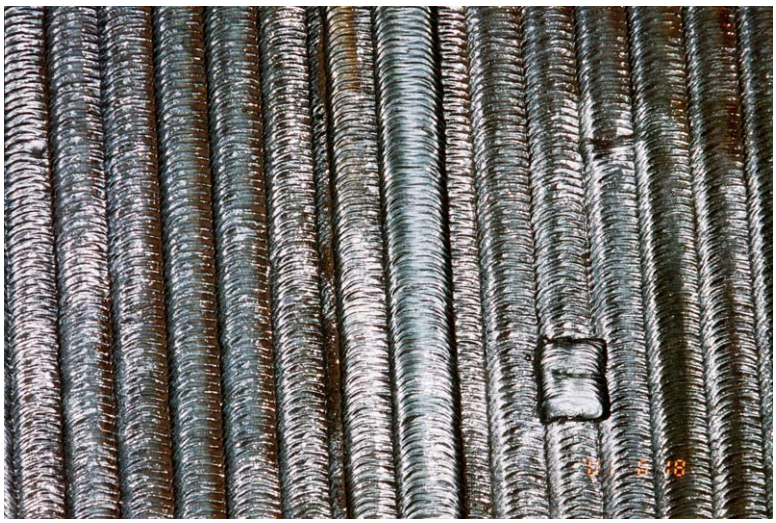

Fig. 15. General region of overlay showing a patch applied to a region where a flaw was detected. June 2001 overlay application.

2.4 ECN PROBES

The probe bodies used in this experiment (see Fig. 16) were fabricated of 316L stainless steel with electrodes embedded in a teflon header. [No composition certification for the 316L probe bodies is available, but by specification limits 316L has 16-18 Cr, 10-14 Ni, 2-3 Mo, <2 Mn, <1 Si, and <0.03 C.] The probe was designed with an adjustable body length so that the surface of the working end could be placed precisely flush with the vessel ID at each probe location. The working end of the probe included two pairs of electrodes representing two materials – mild steel (type 1020) similar to the vessel construction material and 309LSi overlay similar to the overlay used on ring sections 5 and 6. The working end of the probe included a centrally located piece of silver to function as the reference electrode. To monitor temperature for each electrode, a thermocouple was located inside the probe about 3 in. behind the teflon header. [The probe design called for the thermocouple to be exposed is a sheath on the working face of the teflon header, but fabrication problems led the manufacturer to move the thermocouple. Additional detail appears in section 3.3.3.]

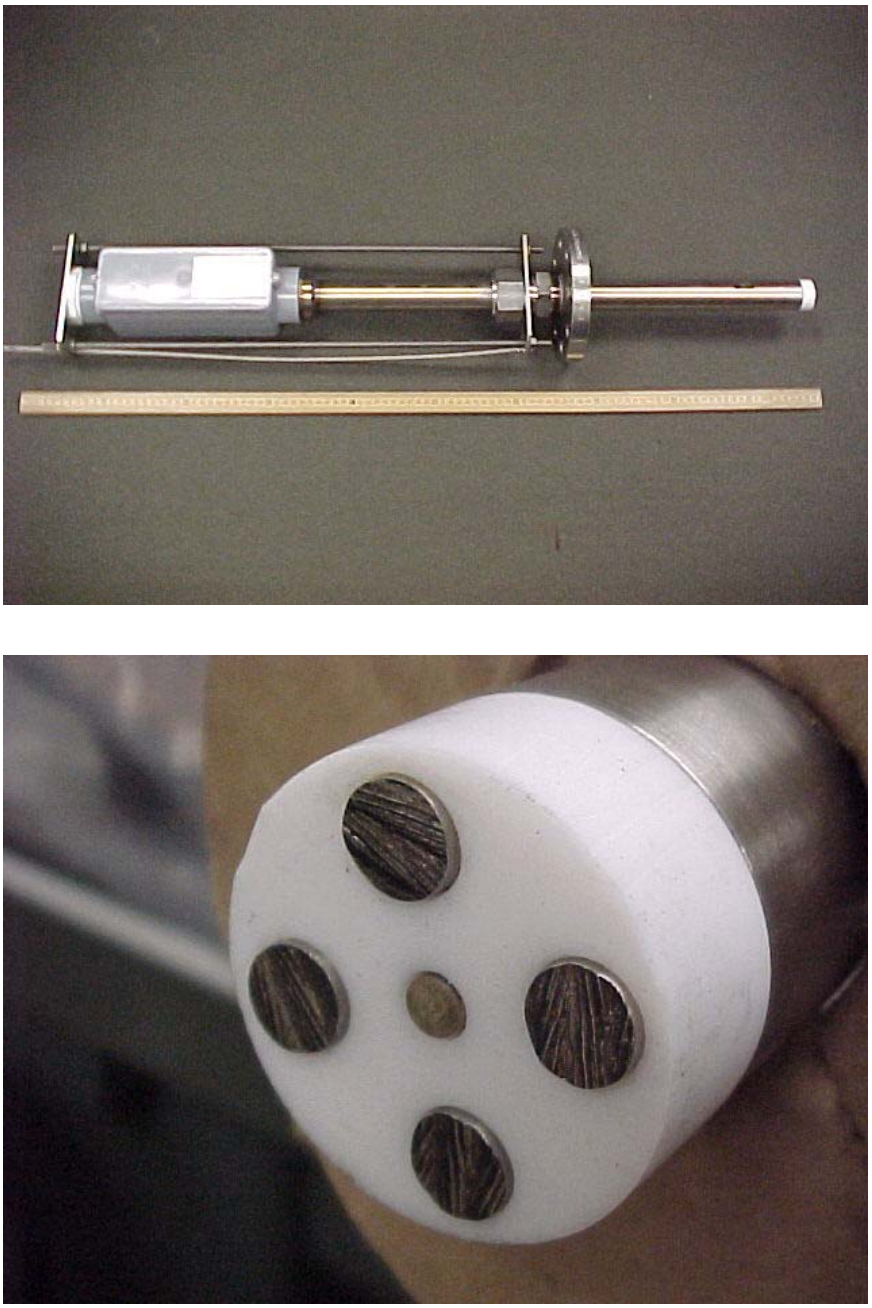

Fig. 16. Adjustable length dual probe used in the Spring Grove experiment. At top, the overall probe is shown. At bottom, a close-up of the teflon header with electrodes is shown. In the probe shown here, all four electrodes are overlay material (two each of types 309LSi and 312 stainless steel, which was the new probe installed at Spring Grove) but for the probes discussed in this report, two electrodes were 309LSi and two were type 1020 mild steel.

Figure 17 shows an installed probe as it appears from outside the vessel. The box at the end of the probe contains the terminal strip for making electrical connections to the electrodes. The wires from each probe run to a central collection point near the digester control room, where the data processing equipment and computer were located.

Fig. 17. View of installed probe (with insulation pulled away). This particular probe is the ring 6N location. The box at the end of the probe contains electrical connections to the electrodes.

Data collection from the probes commenced in late June 2001 following the major maintenance outage, and continued with only minor exception until the following major maintenance outage at the beginning of June 2002. The gaps in data gathering include a shutdown of about two weeks during late December 2001 and early January 2002 as well as a few brief periods early in the experiment in which the data gathering and transfer routine experienced a few problems.

Current and potential values were collected at intervals of one second for each probe. The system hardware included an 8-channel monitoring rack(*) with a standard laptop computer using corrosion software(†) designed for this type of data collection. Statistical parameters (averages, standard deviations, root-mean-square values) were calculated at five-minute intervals. Raw data was discarded approximately every two weeks and only the calculated parameters were saved. The analysis discussed here uses only five-minute averages calculated from current and potential noise for each time interval. The probe thermocouples gathered data on 60-second intervals. In addition, bulk process data (for example, flow rates, temperatures, pump speeds, and liquor composition) from about 30 sensors was collected on approximately 15-30 minute intervals over the duration of the experiment. Particularly for liquor chemistry, measurements were sometimes gathered only 2-3 times per 8-h shift, but some process data was recorded continuously (many times per minute).

The 309LSi overlay electrodes were fabricated from actual overlay material. Type 309LSi meeting the same composition specification as that used in the field at Spring Grove was used to deposit 3/16 in. thick overlay on a substrate of mild steel. [While the weld deposit parameters are not precisely known to the authors, the company making the test material was the same company that applied the actual overlay, so weld parameters should have been very similar. The composition specification for 309LSi includes 23-25 Cr, 12-14 Ni, 1.0-2.5 Mn, 0.65-1.0 Si, 0.03 max C, P, and S, and 0.75 max Cu.] Specimens were then machined from the overlay material, leaving the as-deposited surface intact so that the electrode surface mimicked the actual overlay surface as well as possible.

Figure 18 shows the digester overlay with average ferrite measurements noted for each vertical weld pass. This result is typical of all the ferrite measurements, which indicate some scatter but with an average value close to 2. The ferrite content of the test specimens of 309LSi averaged closer to 9, suggesting a slightly higher Cr/Ni ratio in the test overlay, which was confirmed by chemical analysis of each overlay. Using the average of several determinations made with an alloy analyzer, the data in Table 2 were generated, and it shows that the actual overlay has somewhat less Cr and Ni than the test overlay. Metallographically,

---

(*) CIS400 control unit with CIS502 current-potential logging and zero-resistance ammeter modules from Petroleum Research and Production, Ltd., in England, and ADAM 4018 8-channel temperature loggers, from Advantech, USA.

(†) Amulet software system, from Corrosion and Condition Control, Ltd. in England.

the ferrite content and distribution in the actual overlay deposit (taken from the core specimens removed to permit placement of the probes) compare favorably with the ferrite content/structure of the test electrodes (see Figs. 19-20) but also indicate a slightly lower ferrite content in the former.

Table 2. Composition of overlay materials (weight %, average of at least four determinations). No Si was detected for either overlay by the alloy analyzer.

Element	Test overlay made in laboratory	Actual overlay in deposited in vessel
Fe	57.9	63.6
Cr	24.3	21.3
Ni	12.1	9.7
Mo	0.19	0.16
Mn	3.9	3.8
V	0.17	0.23

Fig. 18. Average ferrite contents (determined by magnetic measurement device) are noted on the crown of each vertical pass of the overlay. The values range from 1-6 in this section.

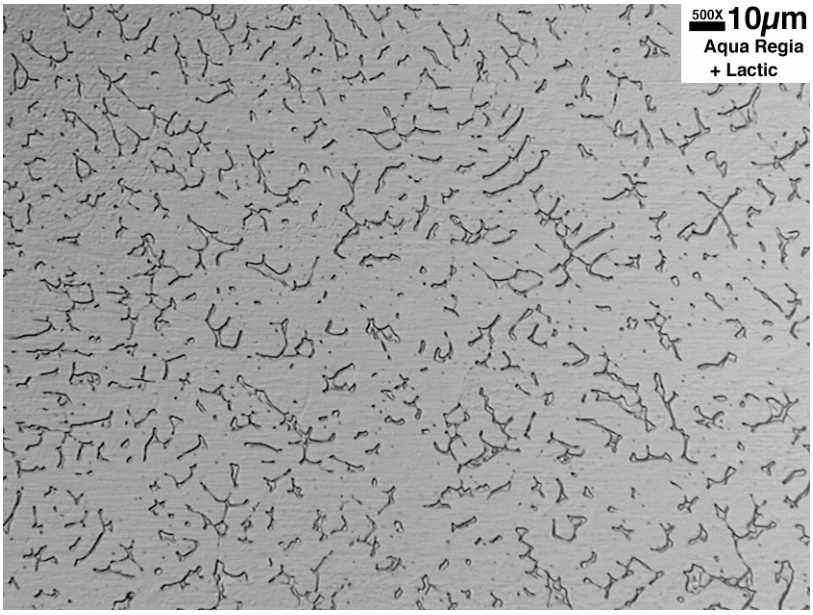

Fig. 19. Cross section of laboratory prepared 309LSi overlay showing residual ferrite in an austenite matrix. The ferrite content and morphology was relatively uniform throughout this specimen.

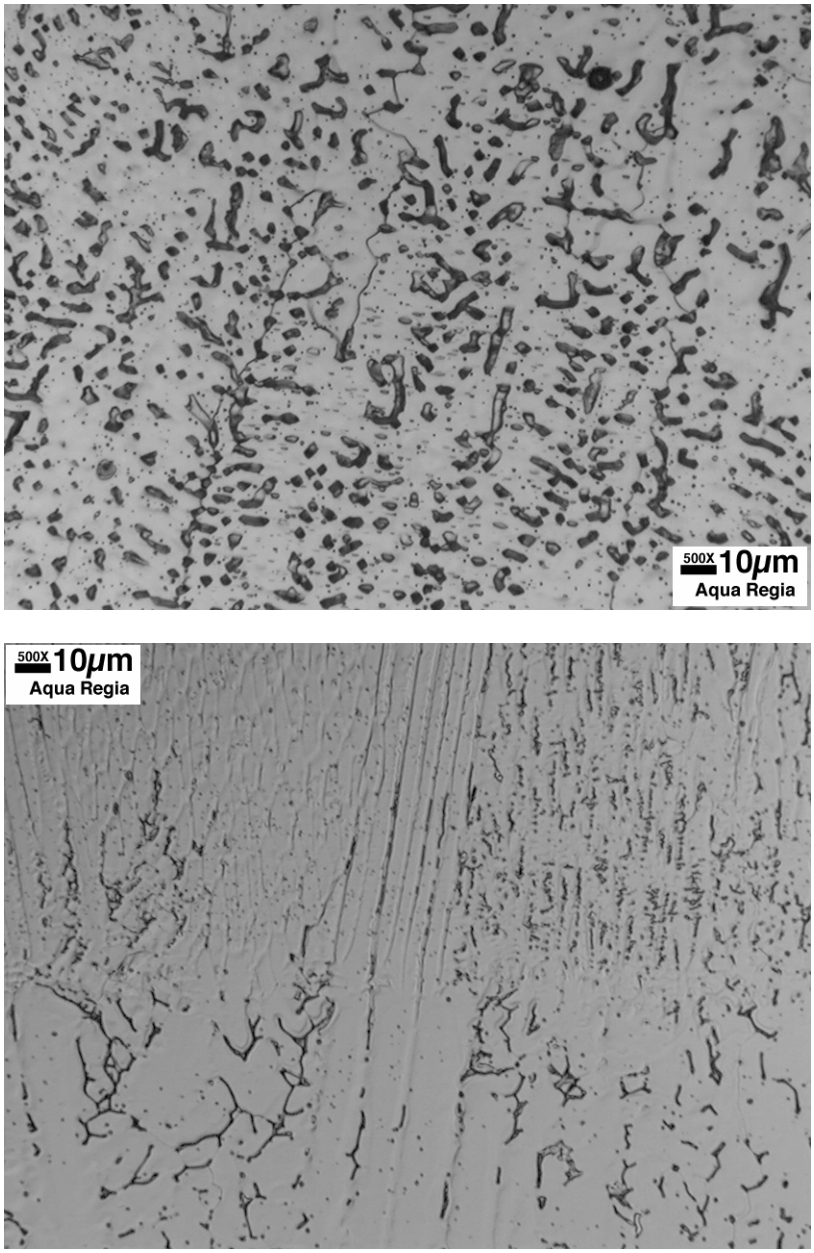

Fig. 20. Cross sections of the 309LSi field weld overlay. The ferrite content and morphology varies significantly in this material as indicated by the pair of micrographs shown here. The relatively low ferrite content shown in the bottom photo is the predominant condition for the field overlay, and appears similar to that of the test overlay (Fig. 19).

3.0 RESULTS AND DISCUSSION

3.1 POST-TEST INSPECTION OF THE DIGESTER

In June 2002, after the ECN probes had been in service for 12 months, the digester was again inspected at the annual maintenance outage. The observations recorded here are organized from the bottom of the vessel to the top. It should be noted that, just prior to the follow-up inspection, additional 309LSi overlay was applied to the bare steel digester shell below the extraction screens such that the entire vessel between extraction and wash screens was overlaid.

Due to the application of the new overlay on rings 3 and 4 at the beginning of the maintenance outage, a photographic record of the condition of the steel surfaces at/around the position of the ring 3 probe immediately after the year-long test period was not collected. Figure 21 shows the region around the ring 3 probe with the new overlay already in place.

Figure 22 shows the intersection of the year-old overlay with the new overlay material. In this lighting, the older overlay has a slightly dull cast compared to the fresh "heat tint" appearance of the new overlay. However, thickness measurements and visual inspection suggest that the overlay in service for one year is essentially unchanged from its as-deposited condition. In particular, the solidification ripples and surface profile of the year-old overlay and the new material are essentially identical.

Figures 23 and 24 show the ring 6N and ring 6S probe ports, respectively. The overlay at this elevation is in generally excellent condition, although in limited areas the sharp detail of the solidification ripples seems slightly lost due to minor erosion/wash. There was no obvious difference in performance of the overlay on the opposite side of the vessel at this elevation.

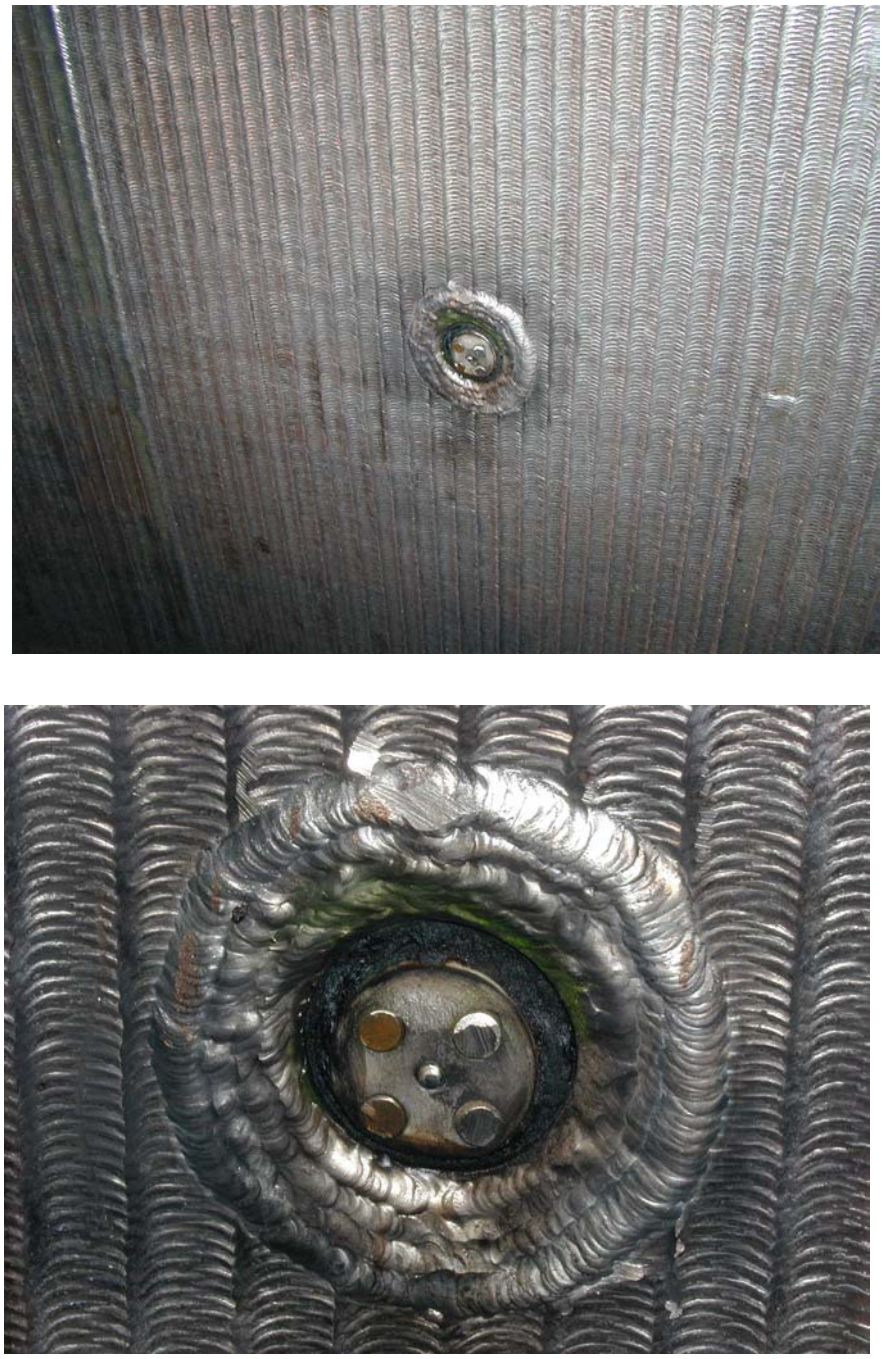

Fig. 21. Digester shell near/around the ring 3 probe following the application of additional 309LSi overlay. Photo from the June 2002 inspection; overlay applied just prior to inspection.

Fig. 22. Intersection of the 309LSi overlay applied on rings 5 and 6 in June 2001 (top portion) with the overlay applied in June 2002 to rings 3 and 4.

Fig. 23. ECN probe in the ring 6N port. Residual black liquor slightly obscures the generally excellent condition of the overlay at this position. Photo from June 2002.

Fig. 24. ECN probe in the ring 6S port. Photo from June 2002.

Figure 25 shows a common corrosion pattern observed on the blank plates in this vessel. Gouges in the shape of a L- or U-shaped fixture (or some other geometric pattern) are common on the blank plates at this elevation. This type of pattern has been observed previously [1] and it seems related to weld heat/grinding activity disrupting mill scale or other passive films in a fashion that accelerates local corrosion. The depth of attack is 60-70 mils deep into the shell ID at these locations. However, the general corrosion on the blank plates at the EX screen level is also significant. At the June 2002 outage, all five rows of blank plates at the EX level were replaced with new plates due to excessive thinning and buckling. Depending on the row from which they were removed, these plates had been in service as much as five years or as little as two years, yet most had areas exhibiting general thinning of more than 180 mils. There was no obvious pattern in the elevation or longitude of the plates exhibiting the most extensive corrosion, and even adjacent plates occasionally revealed a much different extent of corrosion.

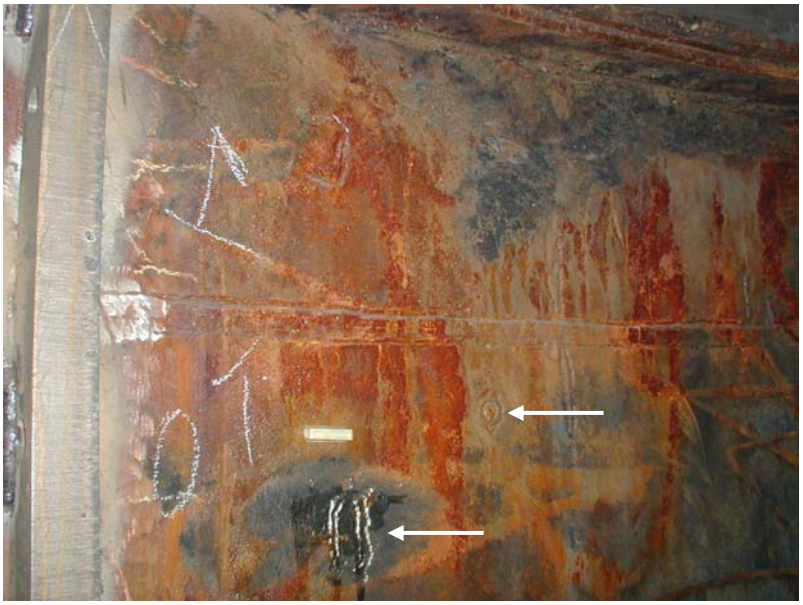

Fig. 25. Blank plate corrosion pattern. The gouge shapes here suggest accelerated corrosion associated with former internal (or present external) attachment positions. The scale marker (white magnetic bar) is 1.5 in. long. Photo from June 2002.

Figure 26 shows a new extraction screen design installed during the 2001 outage. The intent is that the angled screen slots improve the wiping action of the chip mass to minimize clogging of the screens.

Fig. 26. New extraction screen design (slots at an angle).

Figure 27 shows the digester shell in the vicinity of the ring 12 probe. The very light surface roughening observed here is unchanged from the previous inspection, and the ultrasonic thickness inspection at this location indicated no change in shell thickness in the past year. Figure 28 shows the center pipe near the elevation of ring 12 and it, too, shows little or no change in the light surface roughening/pitting pattern observed the previous June.

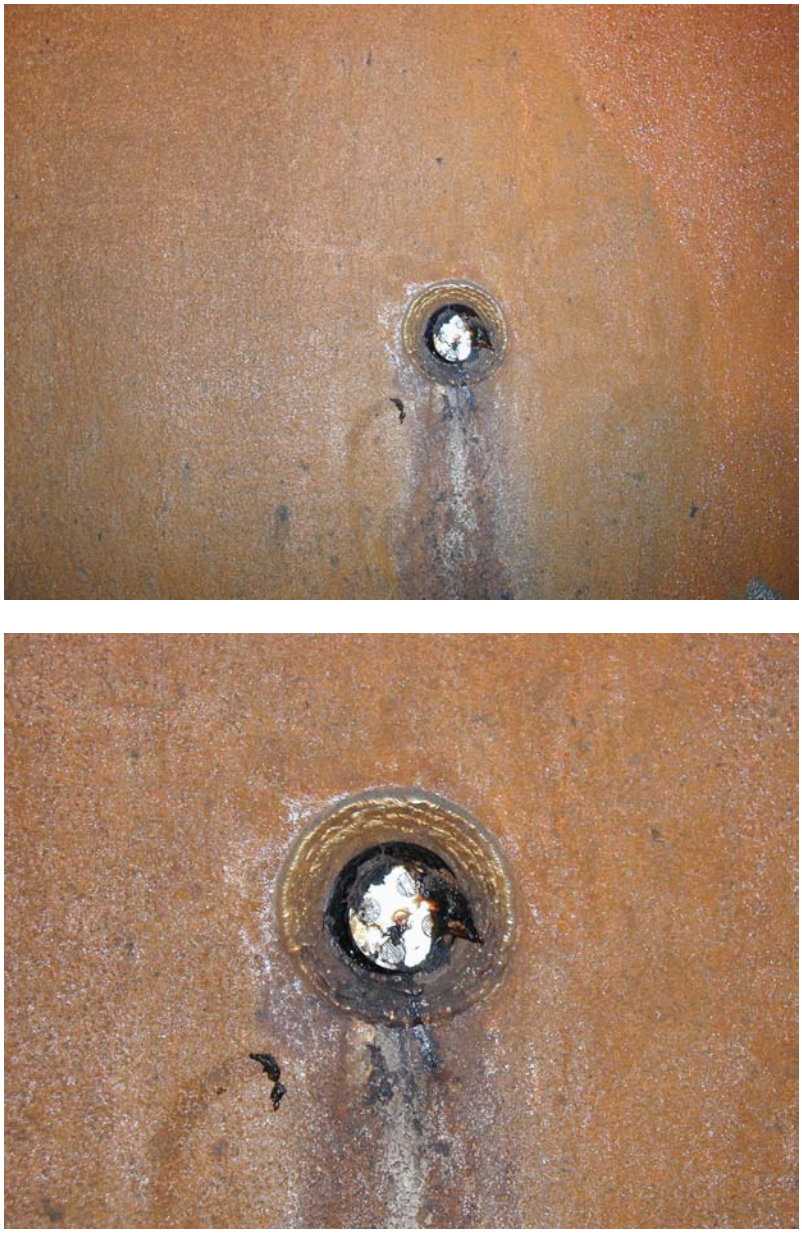

Fig. 27. ECN probe at ring 12 port. Top: general view. Bottom: close-up. The shell corrosion pattern adjacent to this probe remains unchanged from the previous inspection. June 2002 photo.

Fig. 28. Center pipe near the elevation of the ring 12 probe. Pits are approximately 20-30 mils deep with a smooth, hemispherical shape and not obviously different from the previous inspection. Scale marker (white magnetic bar) is 1.5 in. long. June 2002 photo.

Figure 29 shows an interesting pattern that was not specifically observed in the previous inspection. On ring 13, the shallow "oceans-and-islands" corrosion pattern generally observed at this elevation of the digester has not become deeper, but there appears to be a specific elevation (almost a line) in which the coarseness of the pattern changes. It is not apparent that this elevation has suffered greater thinning than the surrounding areas, but the indication appears similar to a high-water mark in a stagnant process.

Fig. 29. The shallow "oceans-and-islands" corrosion pattern appears more intense at this location on ring 13. June 2002 photo. Scale marker (white magnetic bar) is 1.5 in. long.

Figure 30 shows the center pipe just below the cooking screens. The pitting pattern here is generally shallow and scattered, but specific rows/patterns of pits suggest a contribution from the handling equipment used to position the center pipe after the most recent repairs. In particular, the nearly linear or helical rows of pits might have formed as a result of damage to the surface/mill scale by handing with the chains used to hoist the center pipe.

Fig. 30. Center pipe just below the cooking screens. Light pitting seems accelerated in patterns suggesting damage to mill scale from the handling chains when the center pipe was lifted into place. Scale marker (white magnetic bar) is 1.5 in. long. June 2002 photo.

3.2 POST-TEST EVALUATION OF ECN PROBES

Following the year-long exposure, the probes were returned to ORNL for evaluation. The probes were photographed and then the individual electrodes were removed by cutting the bottom of the teflon header and pressing the electrodes free of the teflon. Subsequently, the dimensions of the individual electrodes were measured and compared with the original dimensions to assess the actual extent of corrosion on each.

Figure 31 shows the working end of the ring 6N probe following the year-long exposure, which included the inhibited acid cleaning received by the vessel internals and light water rinsing. The 309LSi electrodes appear largely unaffected by the exposure, but it is clear that the mild steel electrodes have some corrosion product accumulation and have been significantly attacked. In addition, the teflon header appears to have faired quite well during the exposure. The absence of attack on the 309LSi specimens is confirmed by the close-up view in Fig. 32 – the surfaces of the electrode exposed to the process remain bright and shiny with the weld solidification ripples retaining much detail. The mild steel electrodes were severely attacked, but as shown in Fig. 33

Fig. 31. Ring 6N probe after one year of exposure. The 309LSi electrodes appear unchanged from the initial condition, but the mild steel electrodes exhibit significant wastage.

Fig. 32. Close-up of 309LSi electrode specimens from ring 6N probe.

Fig. 33. Close-up of the mild steel electrode specimens from ring 6N probe. The steel electrode on the right has a crater-like profile over a portion of the surface rather than being flat.

the attack appears to be completely general as opposed to localized attack. One of the steel electrodes from this probe suffered perfectly uniform attack decreasing the length of the electrode by about 75 mils, resulting in a flat profile on the electrode surface. The other steel electrode suffered a similar type/extent of attack, except that a portion of the electrode surface (about 25%) has a profile resembling the sides of a crater. The flat portion of this specimen was thinned by 80-85 mils, but the highest edges of the crater suffered only about 45 mils corrosion.

Figure 34 emphasizes the difference in thinning experienced by the two electrode materials in the ring 6N probe. The steel specimen on the left is 80 mils shorter than the 309LSi specimen on the right.

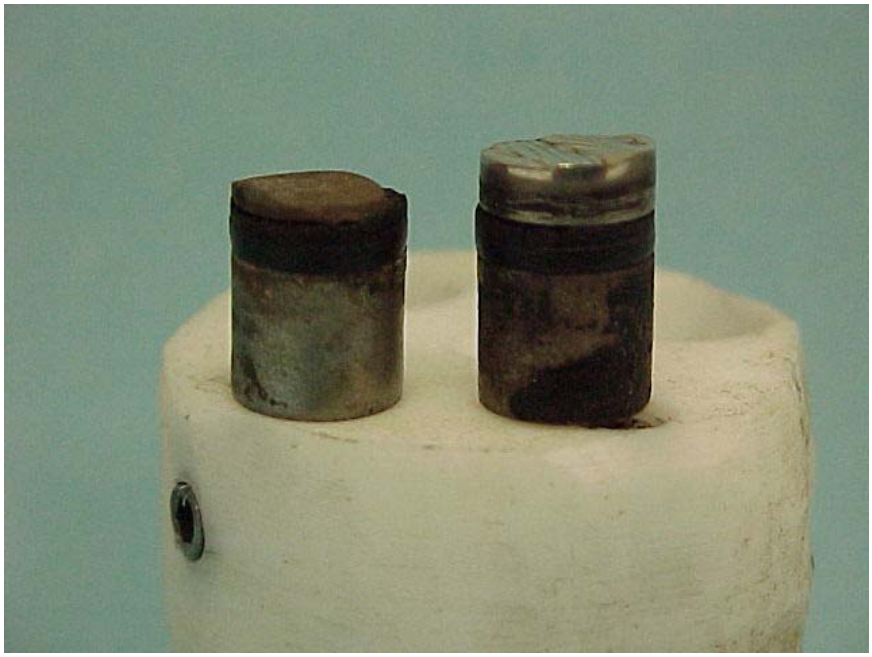

Fig. 34. Length comparison of ring 6N electrodes. The mild steel on the left has suffered about 80 mils more corrosion than the 309LSi electrode on the right.

The appearance of the 309LSi electrodes was the same for all of the probes – rich detail from the original solidification structure was retained on a bright and shiny surface. The attack on the carbon steel electrodes was uniform and general in nature on all the other probes, with the ring 6N probe experiencing the most attack and ring 12 the least.

Table 3 below records the dimensional changes associated with each electrode material as a result of the year-long exposure. In each case, the average of the length and diameter change for the electrode pair is given, but only the steel specimens from the ring 6N probe were not identical to each other. In the case of the ring 6N steel electrodes, as mentioned above, only about 75% of one of the specimens was essentially the same as the other specimen; in this case, the average corrosion recorded is based on the greatest extent of change.

Table 3. Dimensional changes for the individual electrode specimens (given in mils) as a result of the 49-week exposure. [39.4 mils = 1 mm]

Probe	Change in length (mils)	Change in diameter (mils)
Ring 12, mild steel	- 2	- 1
Ring 6N, mild steel	- 80	- 33
Ring 6S, mild steel	- 48	- 26
Ring 3, mild steel	- 19	- 8
Flash tank, mild steel	- 7	- 3
Ring 12, 309LSi overlay	0	0
Ring 6N, 309LSi overlay	0	0
Ring 6S, 309LSi overlay	0	0
Ring 3, 309LSi overlay	0	0
Flash tank, 309LSi overlay	0	0

3.3 REPRESENTATIVE ECN AND OPERATIONAL DATA

3.3.1 Data Analysis and Interpretation

The ECN data collected over the entire year-long experiment was examined in an attempt to find specific events or periods of time in which probe corrosion – and therefore digester shell corrosion – changes from the nominal level of activity. Ultimately, the goal of the effort is to correlate changes in corrosion activity with specific operational characteristics of the digester and identify conditions contributing significantly to accelerated corrosion.

For the present experiment, the data was evaluated for such changes/events in two ways. Primarily, the electrode potential and current activity were examined graphically as a function of time (generally 6-10 week segments) to look for significant/sustained changes in electrode potential or current activity. Time periods in which these changes were detected were compared to graphical representations of each of the operational variables (temperatures, flow rates, liquor composition, etc.) that are tracked and recorded by the mill. In this fashion, an attempt was made to correlate periods of relatively high corrosion activity with specific operational variables. In addition to using graphical trends to identify periods of corrosion activity corresponding to changes in operational parameters, the data was also evaluated via

correlation coefficient analysis for all pairs of process variables with several delay times considered. [This analysis is described more fully in a subsequent section.]

The value of current generated by the ECN probes is a complex – and not necessarily straightforward – number. The current value in any sampling interval is the net current detected flowing through the zero-resistance ammeter (ZRA) connecting the nominally identical working electrodes. Depending on which electrode is momentarily active compared to the other electrode, current can flow from electrode A toward electrode B as well as in the opposite direction. As a result, ECN current can be either "positive" or "negative" with – for the present discussion – no particular significance attached to the sign of the current flow.

Several factors influence the magnitude of the current detected by the ZRA. For example, in any corrosion reaction, there are necessarily areas of both anodic and cathodic activity. If an individual working electrode is sufficiently large, at least some of the corrosion current will be consumed on the surface of the electrode (discreet anodes and cathodes on the same surface) and thus a portion of the corrosion current does not pass through the ZRA and is not detected by the system. In principle, electrode size is an important design feature of an ECN system, with some balance required between the advantages of relatively large electrodes and very small ones. Larger electrodes come closer to representing real surfaces (inclusions, surface roughness, surface deposits/films, composition gradients, etc.) than do small electrodes, but as the surface area of the electrodes increases, the likelihood that the corrosion current self-terminates (anodes and cathodes on the same surface) also increases. Further, the expected signal-to-noise ratio may influence electrode size requirements; for example, a strongly passive system might require a very large electrode surface to generate the required signal. Finally, for pulping liquor corrosion, another electrode size/condition factor might be how readily various reactions which do not directly contribute to the corrosion reaction take place. For example, reduction/oxidation reactions (termed redox, hereafter) involving sulfur species may contribute some electrons detected by the ZRA without directly participating in corrosion of the steel vessel. As long as the electrodes are reasonably similar to the structure they are to simulate (similar roughness, composition, film catalytic effects), it is assumed – for this discussion – the amount of indirect contribution is essentially constant and in the "white noise" of current activity (meaning equal probability of happening on either electrode and thus a factor that largely "cancels" from the current measurement).

Ultimately, there is no known relationship to determine a precise electrode size that is most appropriate for a given system. The literature is replete with examples of successful ECN applications with electrode sizes between 0.5 and 5 cm^2 and there is no reason to expect that such a size is inappropriate for the present experiments. The electrode size chosen for the ECN probes deployed at Spring Grove represents the largest collection of working surfaces (four working electrodes and a reference electrode) that could be fit onto a 1.5 in. (38-mm) diameter probe that mated into a flanged port cut into the digester. [The thermocouple, originally intended to be on the working face of the probe, was instead placed about three inches behind the face of the teflon probe header.]

In this research, the ECN current is typically analyzed/plotted as the absolute value of the current detected by the ZRA. Nominally, the ECN current signal oscillates in a largely random fashion about the value of zero (net current flows back and forth between nominally identical electrode surfaces). However, as the magnitude (not the sign) of current activity is of prime importance to identify operational parameters causing increases in general corrosion activity, the absolute value of current is often plotted for ease of presentation. In particular, when the ECN signals suggest a general corrosion mechanism, the relative sign of the current has no significance. In the case of pitting or stress-corrosion cracking, the sign of the current (indicating a particular electrode) can be part of the interpretation. The corrosion activity in the Spring Grove digester, at least during the period of this test, was exclusively general corrosion. More on that topic appears in discussion to follow.

The sums of absolute current over a specific period of time can be related – albeit in a somewhat crude fashion – to the corrosion rate experienced by the probes (and, in principle, the nearby digester wall). In order to develop such a relationship, certain simplifying assumptions are required. First, the total current must be consumed uniformly over the entire exposed surface area of each pair of electrodes (in this case, 1.24 cm^2 of steel and 1.24 cm^2 of 309LSi overlay for each probe). Essentially, this means that no localized corrosion – such as pitting or stress-corrosion cracking – is occurring (confirmed with post-test analysis of probes) and therefore current is related directly to thinning via general corrosion. In order to relate the current to mass loss and uniform thinning, it was assumed that the iron oxidizes from Fe to the Fe^{+2} state in all cases. Using these assumptions, the total current flow (summed in absolute value) over any period can be related to corrosion rate via Faraday's Law (see Appendix A). Since not all the current for any reaction passes through the ZRA, and some amount of the

current that does pass through the ZRA is related to redox reactions, the value so calculated essentially represents only a fraction, or a qualitative estimate, of the actual corrosion rate experienced by the probes (and digester shell).

3.3.2 General Characteristics

The ECN probes were in place and exposed to the process for essentially an entire year but, due to some problems in the data gathering/archive routine, several weeks of data were intermittently lost during the first three months of the experiment. Beginning in late September 2002, however, data gathering was more efficient and except for a planned mill shutdown and sporadic gaps of 1-2 days, data collection was continuous through the remainder of the experiment. In total, most of the electrode pairs collected data for 253 days. However, in March 2002, the Ring 12 probe was disconnected and the probe in the flash tank was connected to the data gathering unit in its place. As a result, the exposure period for the Ring 12 probe and the flash tank probe sum to 253 days.

Discussion of the data is best served by beginning with a summary of the overall results. Table 4 compares the corrosion rate calculated for each probe material (based on total current passed through the ZRA for each electrode pair normalized to one year of exposure) with the actual corrosion rate observed from post-test measurements of the electrode length (data from Table 3 normalized to a one-year exposure).

Table 4. Comparison of corrosion rates calculated from current sums with those calculated from dimensional changes. Values normalized to one year exposure.

Probe location and material	Corrosion rate (mils/y) calculated from current sums	Corrosion rate (mils/y) determined from dimensional changes
ring 12 carbon steel	2	2
ring 6 – north carbon steel	14	85
ring 6 - south carbon steel	6	51
ring 3 carbon steel	5	20
flash tank carbon steel	9	7
ring 12 309LSi overlay	1	0
ring 6 - north 309LSi overlay	1	0
ring 6 -south 309LSi overlay	10	0
ring 3 309LSi overlay	9	0
flash tank 309LSi overlay	9	0

Unlike the Kamloops digester, in which the agreement between actual and calculated corrosion was quite good [1], the data in Table 4 indicate agreement for calculated (current sum) and measured (dimension change) values of corrosion rate is poor for the steel electrodes. On a qualitative basis, the highest and lowest calculated corrosion rates correspond to the highest and lowest measured rates, respectively. However, the intermediate values exhibit no particular qualitative pattern. It is also noteworthy that the actual wastage experienced by the electrodes at the ring 6 and ring 3 positions was considerably higher than any previously documented rate of digester wall thinning at these positions, suggesting that conditions in the digester leading to accelerated corrosion of steel have not only changed in the recent past but perhaps are continuing to change in a way that is more aggressive toward steel.

For the 309LSi stainless steel overlay electrodes, the electrodes physically exhibited nil corrosion while the current sums indicated some modest corrosion activity. Apparently, the passive film on the stainless steel was very protective for these pulping conditions and perhaps supported a redox reaction on the surface to a degree at least qualitatively suggested by the current sum values at each position. It is interesting that the very different behavior observed in the digester at the positions of the ring 6 probes (north side physically corrodes more than south side) is also revealed in the very different current sums associated with the stainless steel overlay electrodes. In the latter case, the large difference in apparent redox activity suggests the presence of a chemistry gradient between the ring 6-north and 6-south positions. For example, it may be that at least one constituent capable of participating in a redox reaction is plentiful in the region of the ring 6-south probe that is not so plentiful at the position of the ring 6-north probe. Alternatively, a constituent present at the ring 6-north position may block the redox reactivity detected by the ring 6-south probe (where the constituent might be absent). As a matter of pure speculation, the similarity in redox activity suggested between the ring 6-south and ring 3 probes may suggest that the source of the chemistry gradient is non-uniform upflow in the digester.

The lack of good agreement between the measured and calculated corrosion rates casts some doubt on the utility of the probes to detect changes in the corrosivity of the environment as a result of variations in operational parameters. Nevertheless, current activity (redox, wastage, or a combination thereof) and potential remain the best monitors of significant environmental changes in the process, and analysis of the data through the year-long experiment was performed in an attempt to correlate corrosion activity and operational variables in real time.

3.3.3 Temperature Measurement

The original design for the ECN probes included a thermocouple placed in the teflon header of the device. However, due to manufacturing difficulties, the thermocouple was instead placed in the stainless steel housing about 3 in. behind the probe face that was exposed flush with the vessel ID to the process. The probe port was larger in diameter than the probe, so process solution and wood chips no doubt reached this location, but at a temperature somewhat lower than the temperature at the working end of each probe. As a result, the

temperatures reported for each probe track changes in the vessel but underestimate the actual values by approximately 30-35°C. For example, the extraction temperature measured at the mill was essentially constant at 165°C for large periods of time with periodic negative deviations, while the ring 6S temperature measurement was consistently 130-135°C with the same periodic negative deviations. [Specific data are reported in Section 3.3.7.]

3.3.4 Carbon Steel Probes – Ring 12

Consistent with the appearance of the digester wall at this location, the carbon steel electrodes at ring 12 exhibited very little corrosion. As a result of limited activity, the ECN behavior of the steel electrodes at ring 12 is relatively straightforward. For example, the steel potential at ring 12 was essentially constant over the duration of the year-long deployment. Early in the experiment, the potential averaged about –15 mv (vs. Ag/Ag_2S) with some modest scatter, but over the next few weeks, the potential drifted gently downward to the range of –40 to –50 mv (vs. Ag/Ag_2S) where, with only limited exceptions, it remained throughout the remainder of the experiment.

Figure 35 is representative of the ECN behavior of the steel at ring 12 early in the experiment. Note that the potential is relatively constant with only two significant deviations. On 6/29, the potential increases to a maximum of about 100 mv greater than the nominal value but has almost no current activity above the baseline level associated with this event. On 7/2, there is even a larger (magnitude and duration) potential increase for which there is a coincident modest current change. Although the absolute value of current is plotted here, it is significant to note that the steel at ring 12 showed no current bias – that is, neither electrode preferentially became anodic to the other and the current fluctuated randomly about the value of zero and continued to do so until very late in the exposure.

In Figure 36, the probe potential and temperature are plotted together to show that neither potential excursion is associated with a substantial temperature change. Further, the average electrode temperature on ring 12 varied only about 1.5°C during the two potential excursions, with the lower average temperature producing the most significant current response. While there are limited exceptions at all probe positions, it was found to be a general trend that the temperature at each probe location is sufficiently constant to have little apparent effect on ECN activity. The potential excursions depicted in Fig. 35 were not correlated to any specific

operational variables tracked at the mill. However, the potential excursion on July 2 was linked to a general shutdown of the digester in which digester pressure briefly deviated to a

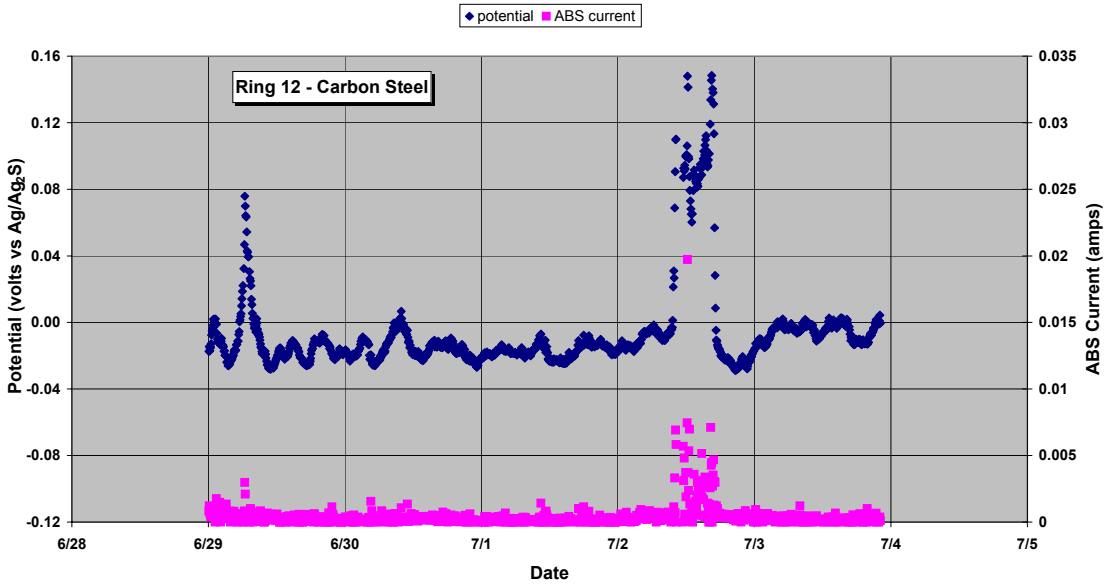

Fig. 35. Representative ECN data for the carbon steel electrodes at ring 12.

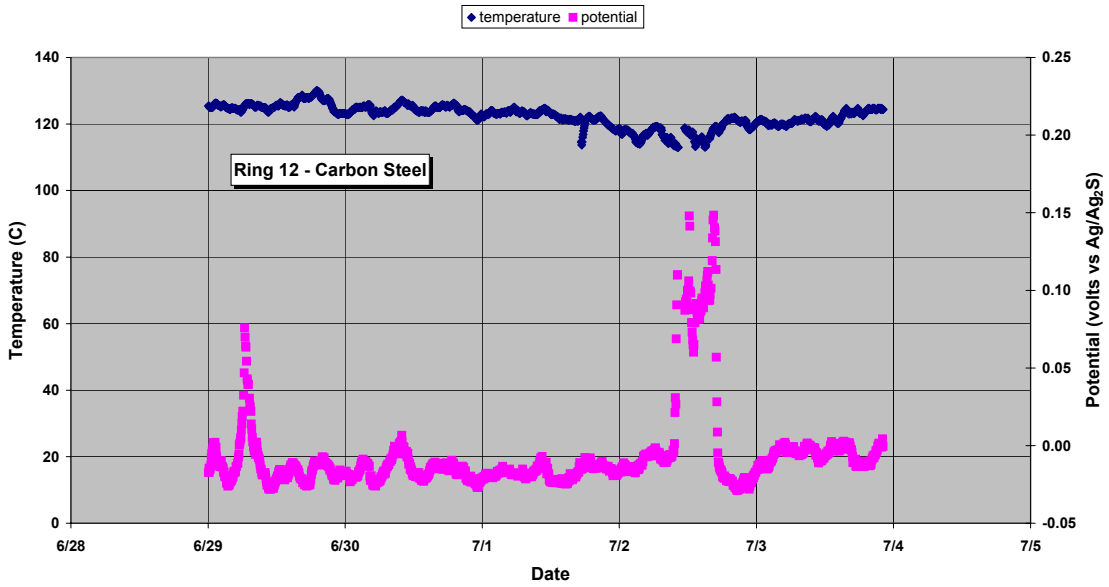

Fig. 36. Temperature and potential plotted together for the same period shown in Fig. 35.

value near half of nominal. Similar sudden but brief changes in many other operational parameters occurred simultaneously with the pressure deviation. Such perturbations are often associated with disruptions of the movement of the chip mass due to chip feed problems, while some of the disruptions were related to brief planned maintenance efforts. Disruptions of this type (in which most/all process variables were perturbed simultaneously) were the most common and reproducible "correlation" among all the process/ECN data examined and occurred perhaps a dozen times over the year-long experiment. Depending on the type and duration of the disruption, repressurization may be required. During repressurization, extreme variations in many process parameters may occur for brief periods, giving rise to unusually aggressive corrosion conditions.

Figure 37 represents ECN data from ring 12 somewhat later in the exposure. With the exception of transients associated with shutdown and start-up of the vessel, this potential excursion is perhaps the largest for ring 12 in terms of combined magnitude and duration. Figure 37 shows that the potential is essentially constant at near –45 mv (vs. Ag/Ag_2S) before and after the steady excursion to a potential near 100 mv above average. During the excursion, the average current per unit time is about double that of the average during the remainder of the period shown, but is nevertheless an insignificant corrosion event. No significant process variable change was identified to coincide with this event, although it is perhaps significant that the stainless steel electrodes at ring 12 also indicated a similar kind of activity change occurring at the same time as that for the steel electrodes. This result perhaps indicates a change in redox activity within the vessel corresponding to a chemistry change that is not monitored in the vessel. Similar to a previous example, Fig. 38 shows that the probe temperature is not likely to be a significant factor in the ECN behavior associated with this excursion.

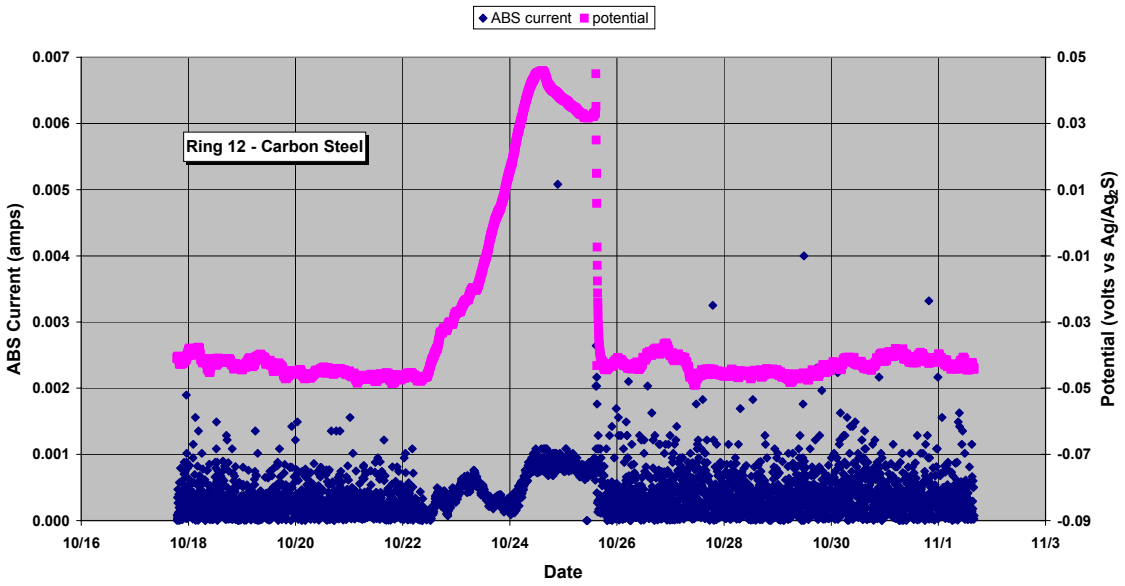

Fig. 37. ECN excursion for the steel electrodes at ring 12.

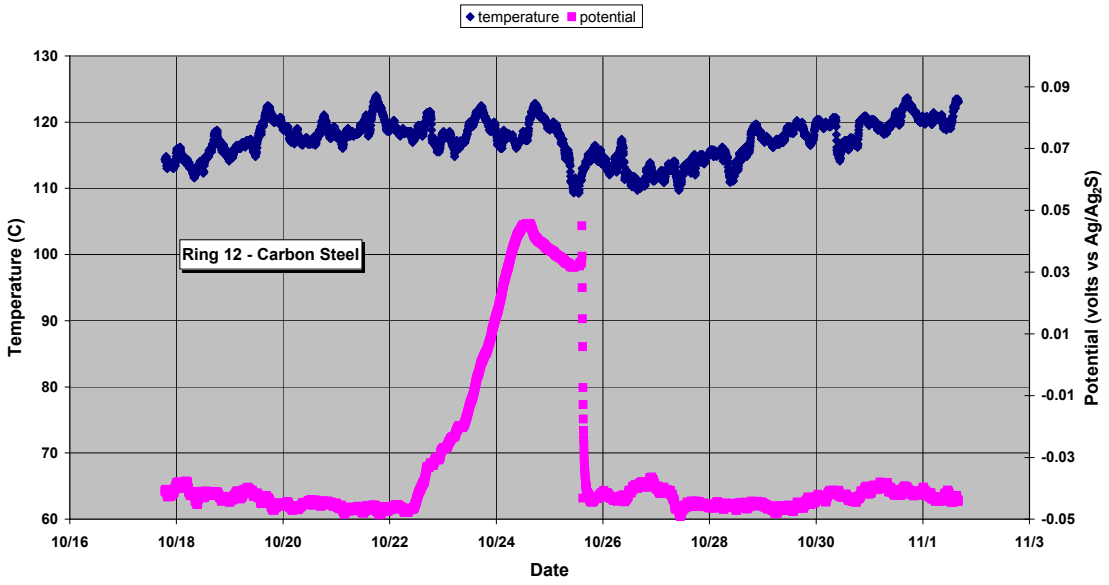

Fig. 38. Temperature and potential plotted together for the same period shown in Fig. 37.

By about four months after start-up, the steel potential at ring 12 became remarkably constant. Figure 39 shows that the steel electrodes at ring 12 had a potential of –50 mv (vs. Ag/Ag_2S) for weeks at a stretch, with essentially zero corrosion current during this time. The excursion beginning on December 21 is associated with a planned shutdown of the vessel. Note that there is a significant potential excursion and current activity associated with the shutdown event. Again, Fig. 40 shows that the nominal temperature variations for the ring 12 probe continue with no effect on potential (and, by inference, current) at least until the shutdown in late December.

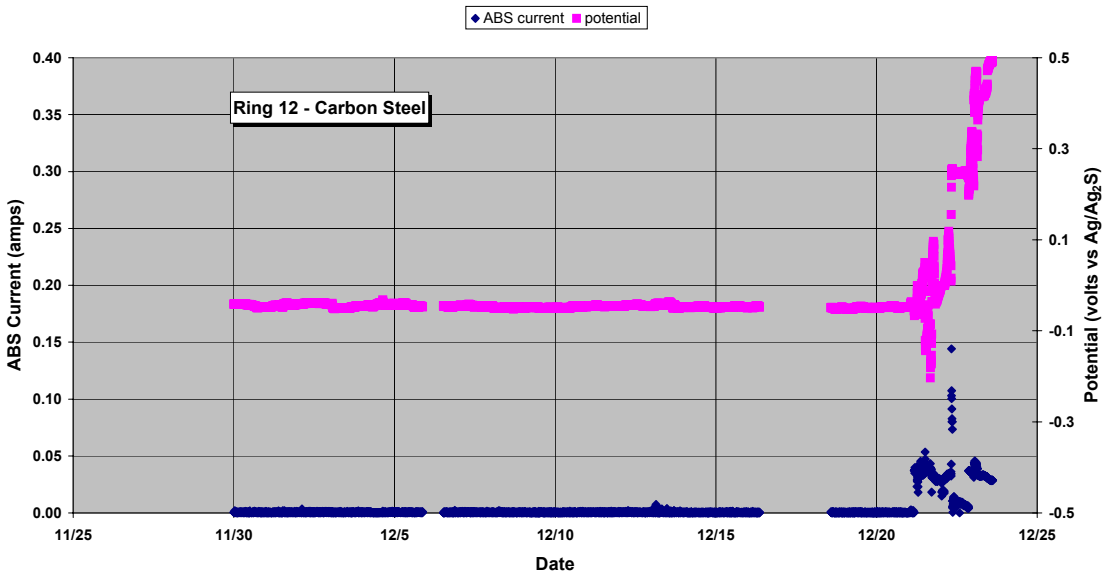

Fig. 39. ECN data for the steel electrodes at ring 12 leading up to the planned outage on December 21.

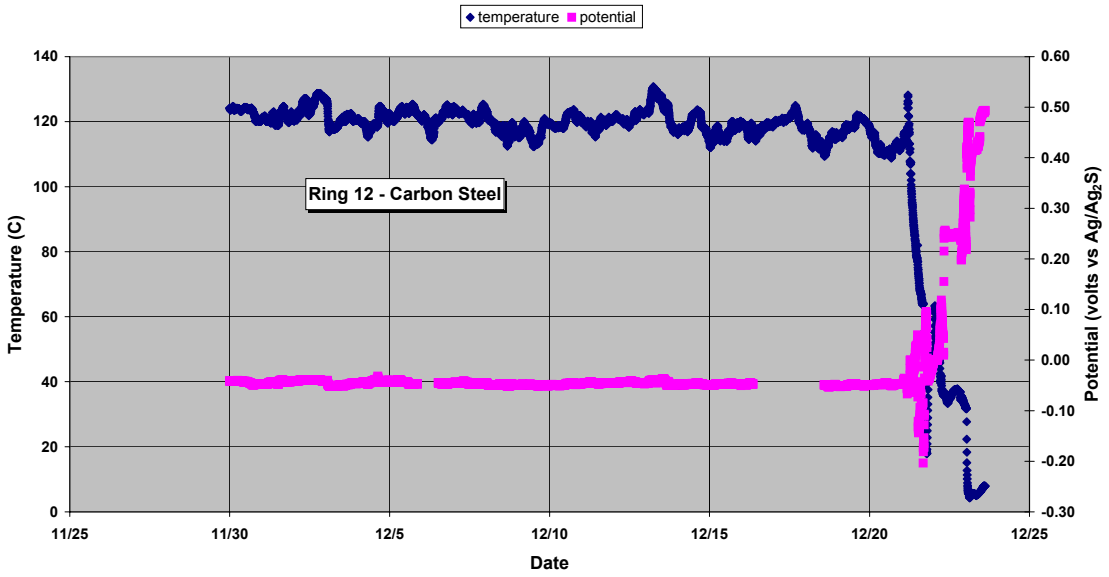

Fig. 40. Temperature and potential plotted together for the same period shown in Fig. 39.

3.3.5 Carbon Steel Probes – Ring 3

Figure 41 is representative of the ECN behavior of the steel electrodes at ring 3 through the first six months of the exposure. The potential varies about ± 40 mv around a numerical average of +51 mv (vs. Ag/Ag_2S) for the period shown. With the exception of a momentary current spike to above 0.02 amps corresponding to the highest potential spike (to +135 mv), none of the potential variations seem to have significant impact on the current noise. Similar to previous examples, Fig. 42 shows that routine potential variations of ± 40 mv or more are often associated with a temperature that is constant within ± 5°C.

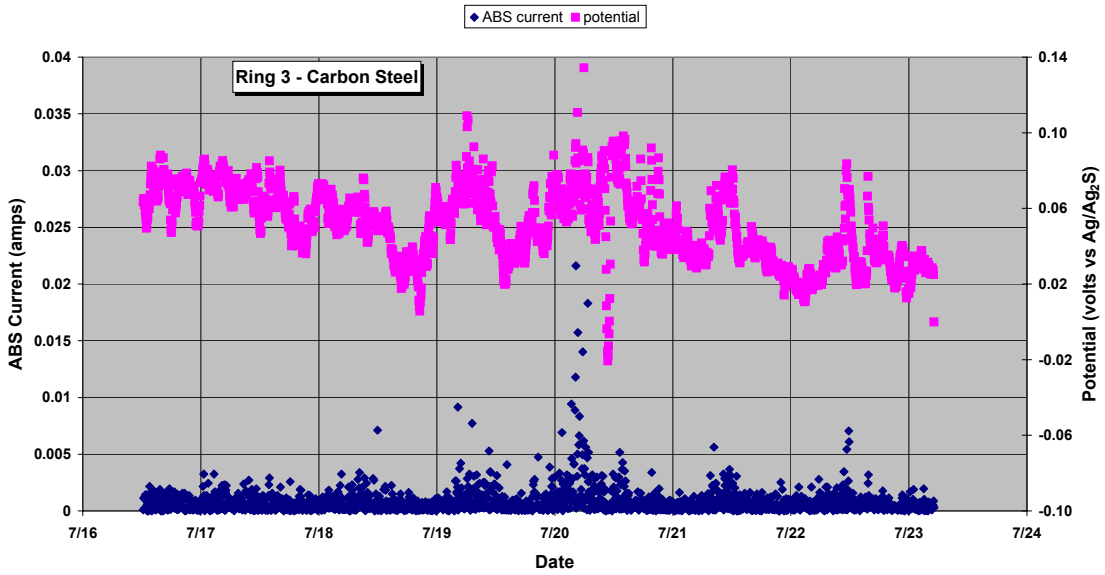

Fig 41. Representative ECN data for the steel electrodes in the ring 3 probe early in the exposure.

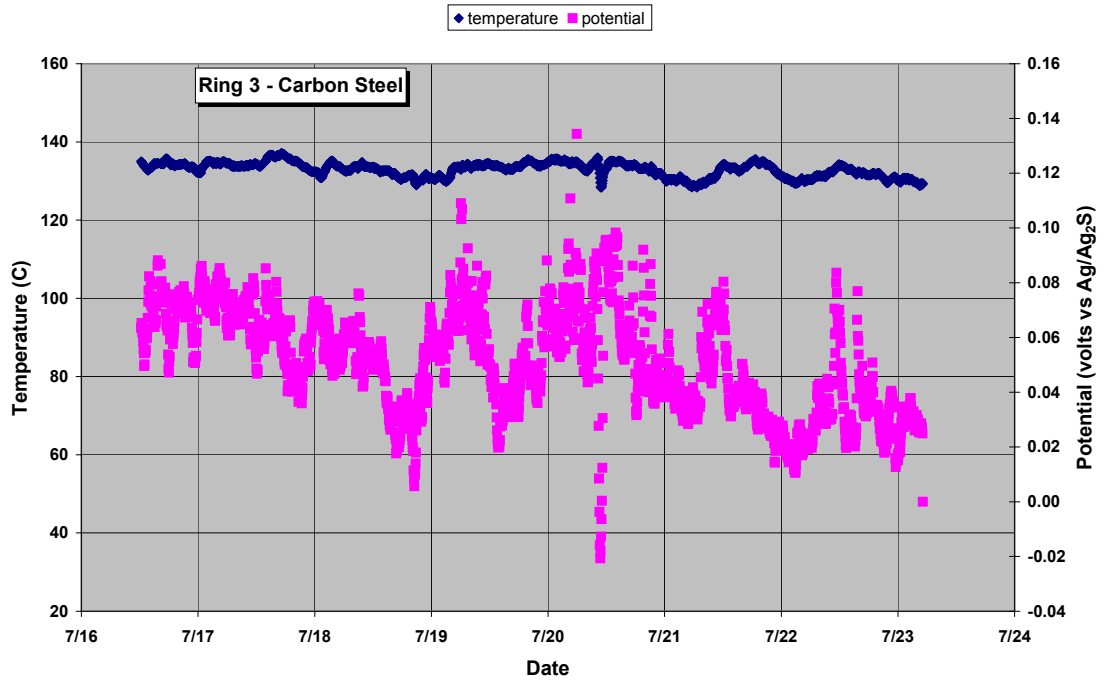

Fig 42. Temperature and potential for ring 3 steel electrodes for the same period as shown in Fig. 41.

Six months into the exposure, the potential of the steel electrodes at ring 3 continued to vary irregularly, but the extremes of the variation, in particular the maximum potential, slowly decreased. Generally, the current noise remained uniform and modest, but increased significantly in magnitude after the start-up in January. On January 5 (see Fig. 43), the steel probes experienced a significant and sustained negative shift in potential (from an average near +40 mv to about zero mv) and a corresponding decrease in current magnitude. No changes in recorded process variables coincide with the sudden potential/current change indicated here. Again, Fig. 44 shows that the change in potential early in January does not appear related to probe temperature.

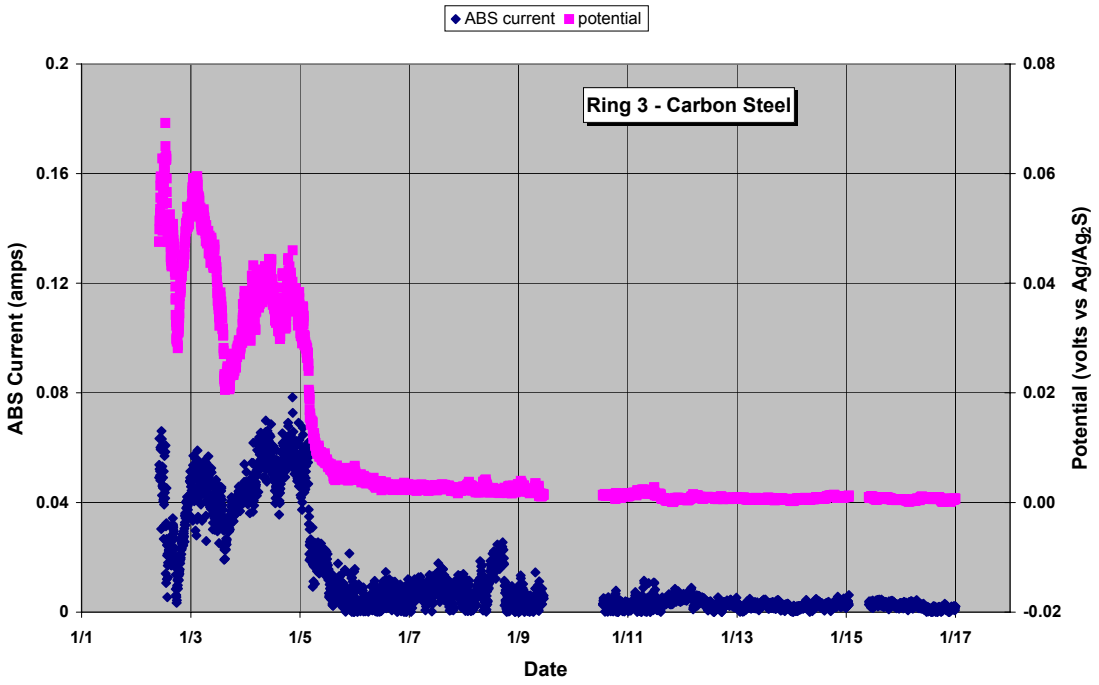

Fig. 43. Representative ECN data for the steel electrodes in the ring 3 probe following the January restart.

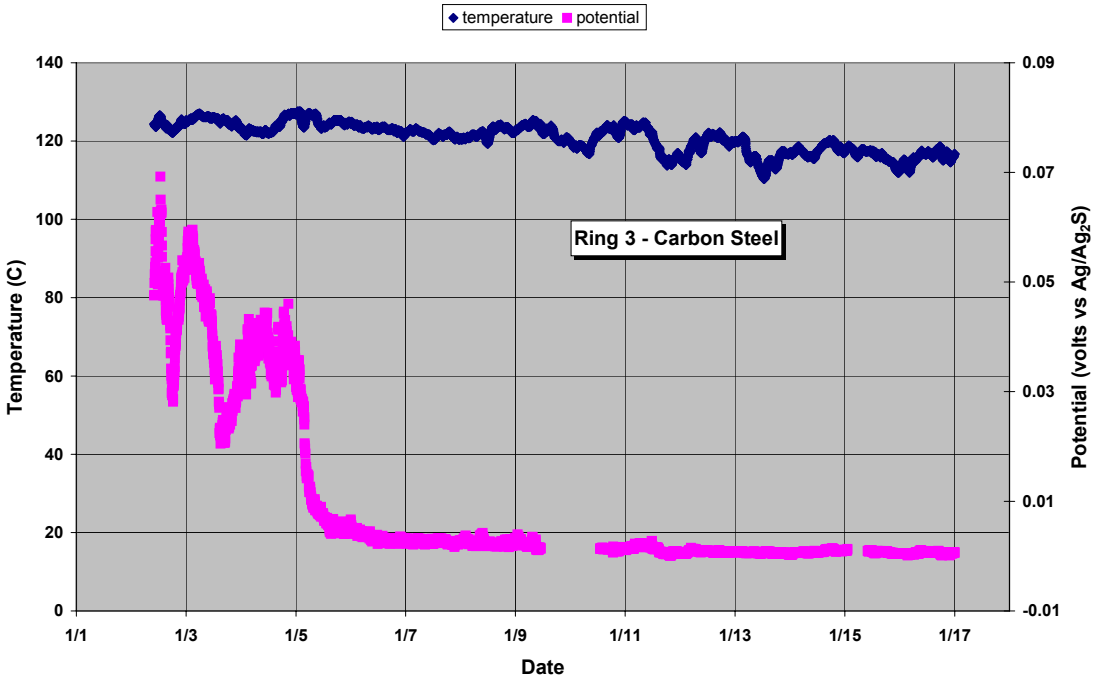

Fig. 44. Temperature and potential for ring 3 steel electrodes for the same period as shown in Fig. 43.

The ECN behavior established on the steel probes at ring 3 in January continued essentially uninterrupted until the digester shutdown in June. Figures 45 and 46 are representative of this behavior, and they reveal modest current demand and few variations in potential greater than about ±5 mv. The modest upset in potential and current noise and particularly probe 3 temperature on May 19-20 is associated with a significant process upset (chip feed problems) in which many process variables changed significantly (but briefly) and all the probes responded with similar potential/current excursions.

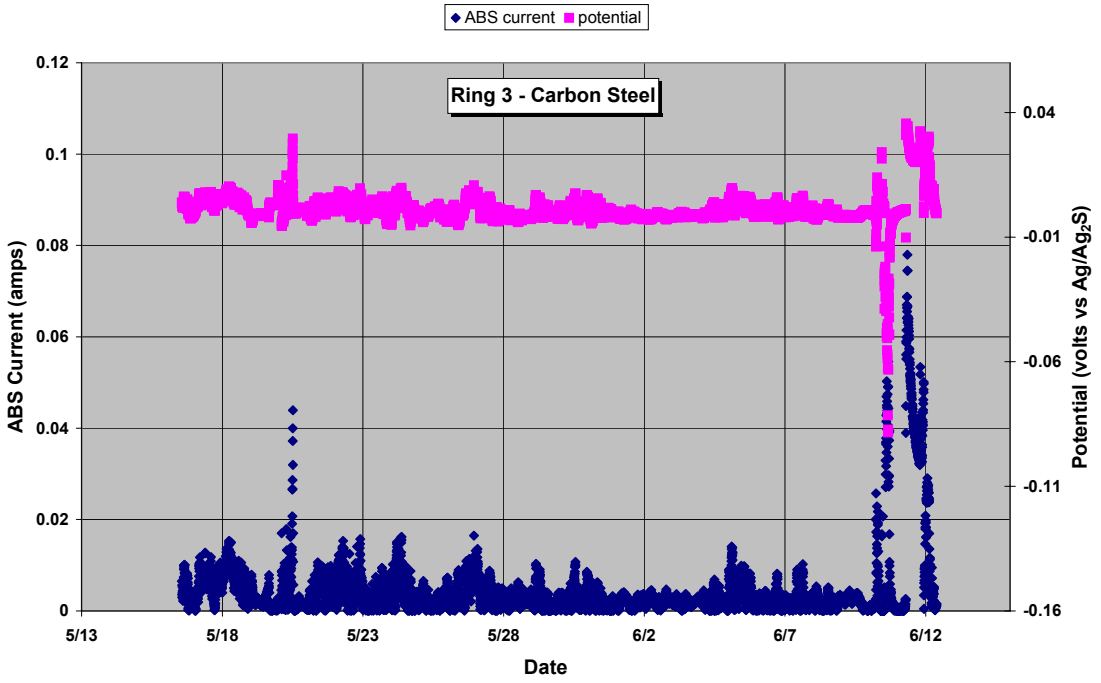

Fig. 45. Representative ECN data for the steel electrodes in the ring 3 probe late in the exposure period.

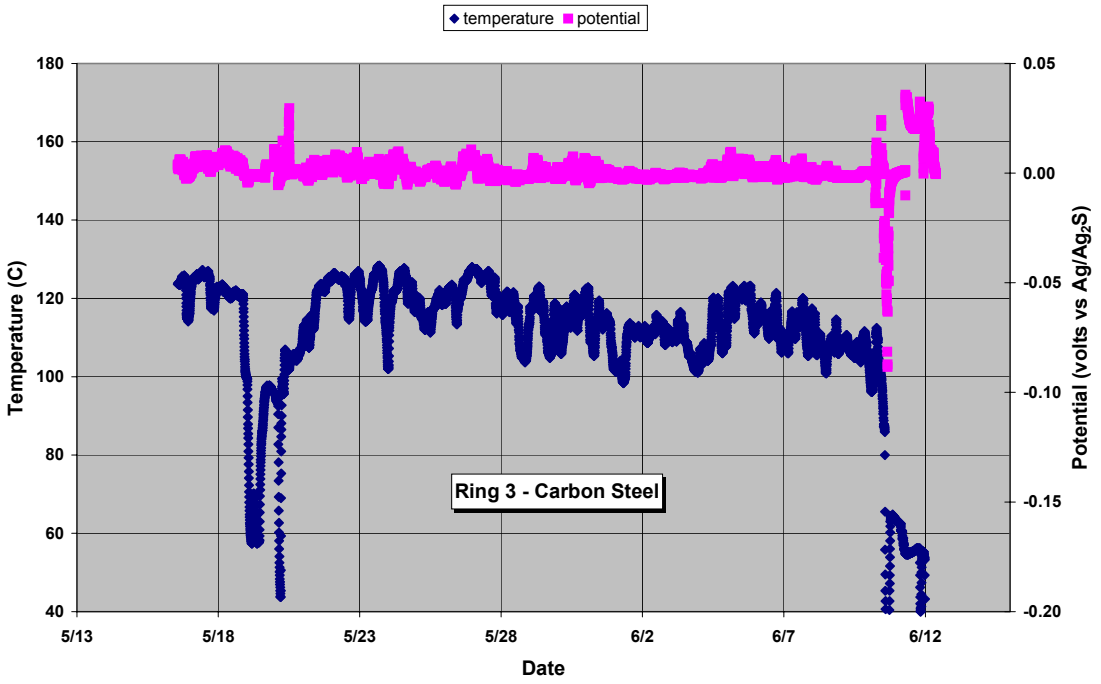

Fig. 46. Temperature and potential for ring 3 steel electrodes for the same period as shown in Fig. 45.

3.3.6 Carbon Steel Probes – Ring 6S

Compared to the potential of the steel electrodes at rings 3 and 12, the potential of the steel at ring 6S is significantly higher over the course of the exposure. Figure 47 shows ring 6S data near the start-up on June 24, and there are three distinct regions in the period shown. In the initial period ending on June 26, the absolute value current sum indicates an average corrosion current of at least 8.9 amps/day and correspondingly high average potential of +205 mv (vs. Ag/Ag_2S). Shortly after start-up, from about June 26 – 28, the average potential drops to –74 mv and the corrosion current drops to an average of 0.6 amps/day. Beginning late on June 28, the steel at ring 6S assumes a more typical ECN behavior observed for the remainder of the period (and the year). The average potential of +87 mv is between the previous extremes as is the average corrosion current of 1.8 amps/day. While temperature data was not available until June 26, it is clear from Fig. 48 that temperature and potential excursions don't follow a particular pattern.

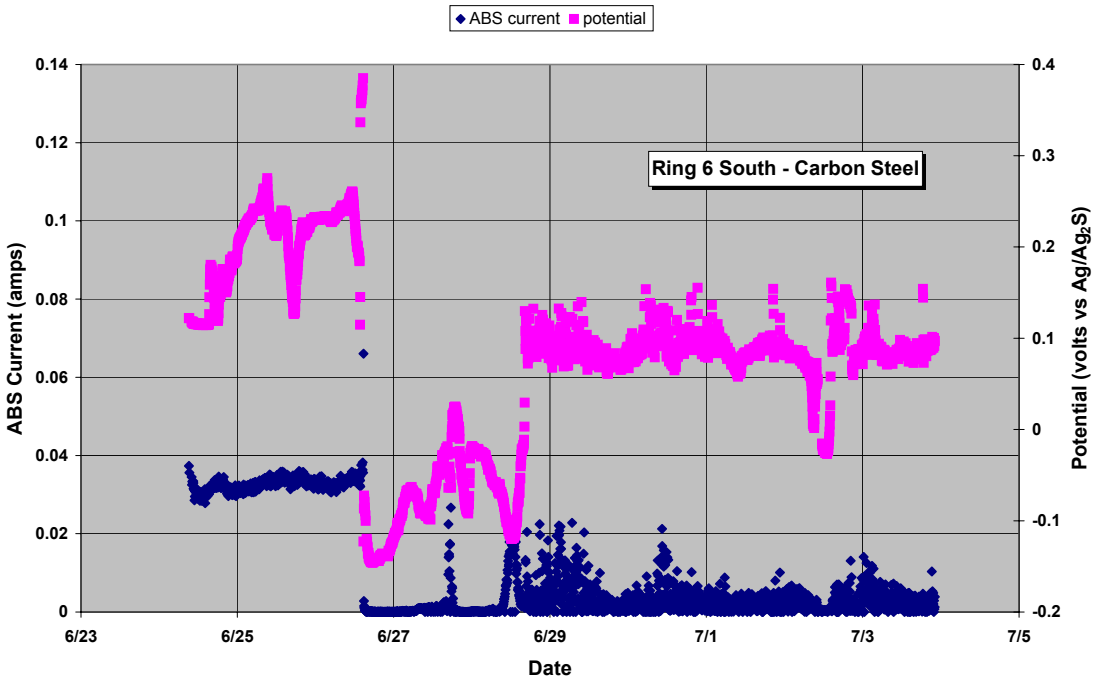

Fig. 47. Representative ECN data for the steel electrodes in the ring 6S probe early in the exposure.

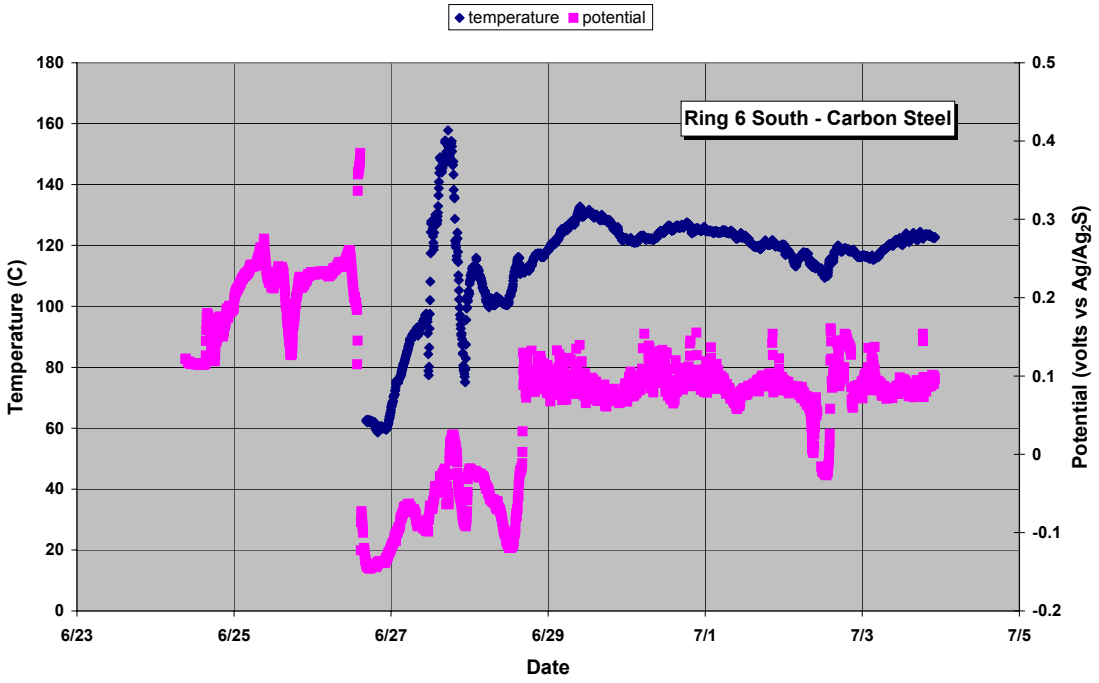

Fig. 48. Temperature and potential for the steel electrodes in the ring 6S probe for the same period as shown in Fig. 47.

Figure 49 is representative of the nominal ECN behavior of the steel at ring 6S after the initial start-up. The average potential maintains significant short-term variation with an average near +80-85 mv (vs. Ag/Ag_2S), but the current sum is lower in this month-long period than any similar period in 2002. In fact, beginning with the period shown in Fig. 49, the current flowing between the steel electrodes at ring 6S approximately doubles in each of the following three months, with no corresponding change in the operational data or average potential. In addition, the ring 6S steel electrodes began to display some current bias (current noise not centered on zero) about nine months into the exposure period. Again, Fig. 50 shows that the potential variations are not directly correlated with the probe temperature. Although not represented graphically, the shutdown in June 2002 exhibited behavior similar to the start-up data shown in Fig. 47.

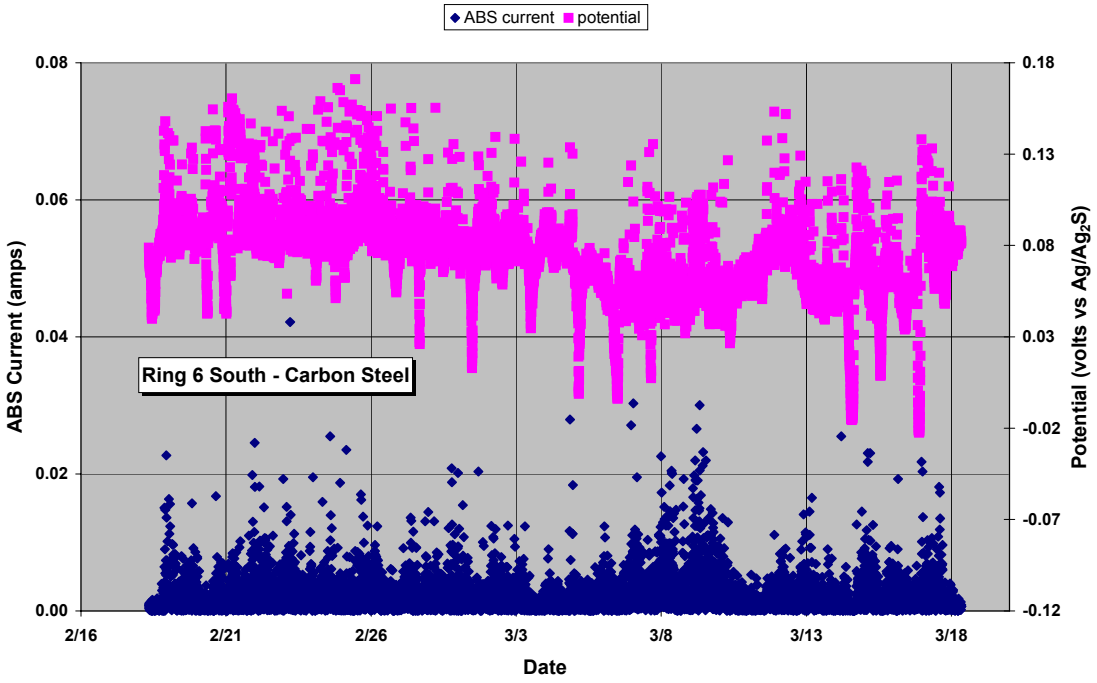

Fig. 49. Representative ECN data for the steel electrodes in the ring 6S probe after the initial start-up.

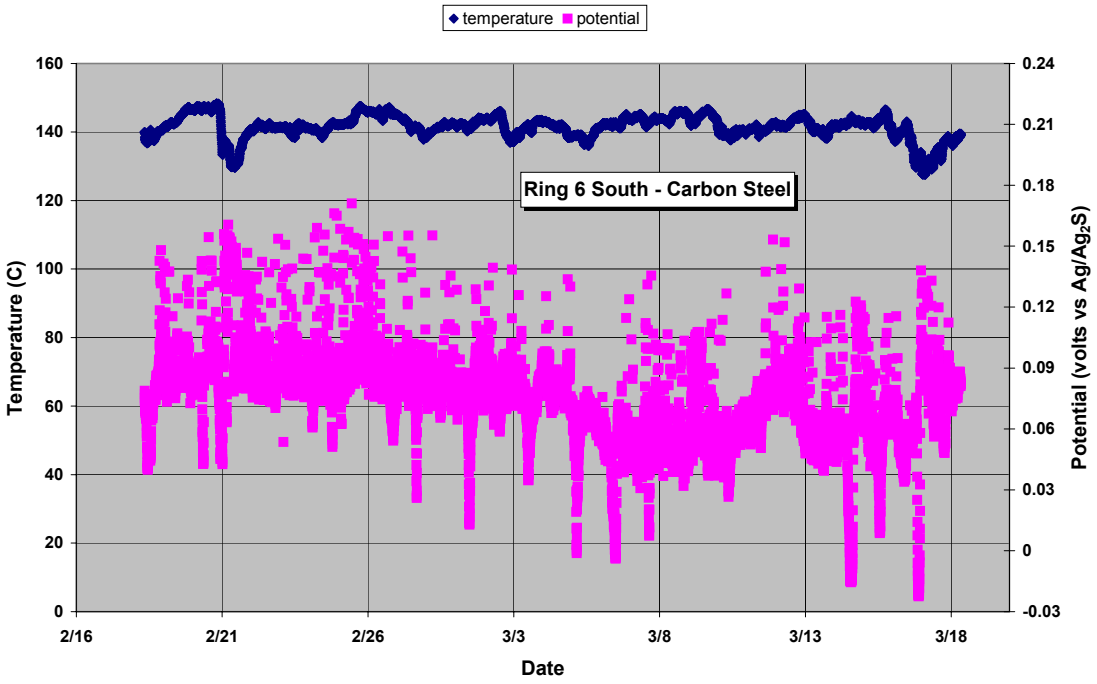

Fig. 50. Temperature and potential for the steel electrodes in the ring 6S probe for the same period as shown in Fig. 49.

3.3.7 Carbon Steel Probes – Ring 6N

The probe at ring 6N was located at the same elevation as that for ring 6S, but 180° away on the opposite side of the vessel. Figure 51 shows that the potential of the steel electrodes at ring 6N is similarly variable but somewhat higher on average than at ring 6S, and the current sum for the period shown is about seven times larger for the steel at 6N than at 6S. There was another month-long period (not shown in Fig. 51) in which the current sum associated with ring 6N activity is a factor of approximately seven larger than for ring 6S, but the average difference over the entire exposure period was closer to a factor of 2.5.

It is interesting that there are two prolonged (>24 h) potential excursions to lower than nominal values shown in Fig. 51. The most severe – on October 13-14 – is associated with a current decrease to near zero. As evident in Fig. 52, this large potential decrease is associated

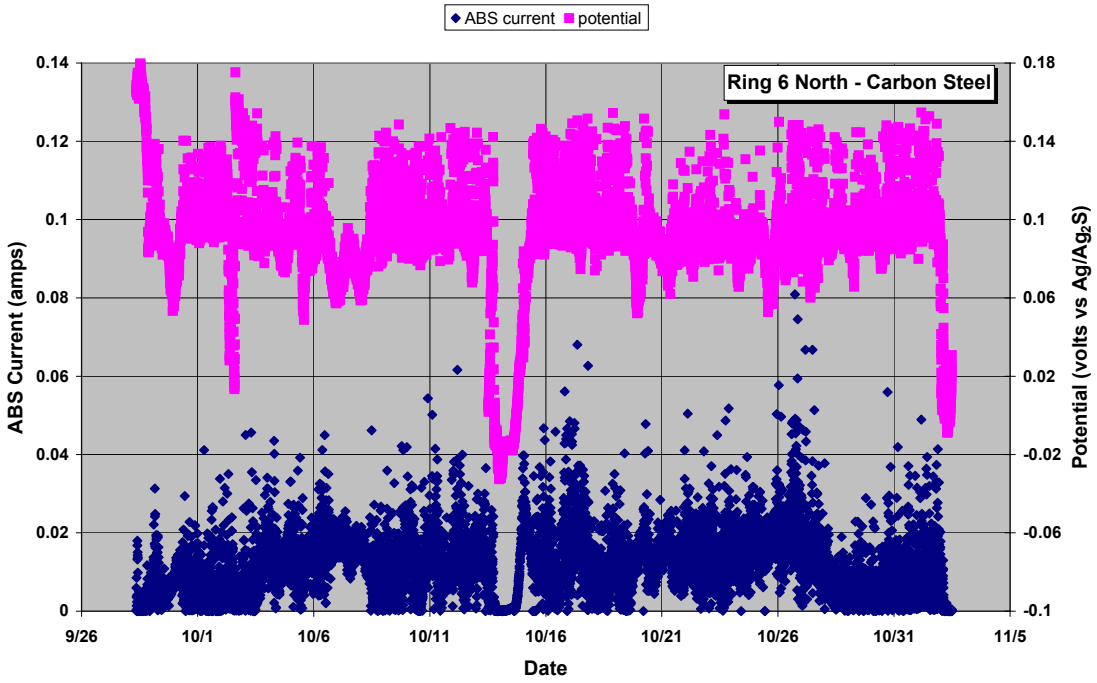

Fig. 51. Representative ECN data for the steel electrodes in the ring 6N probe.

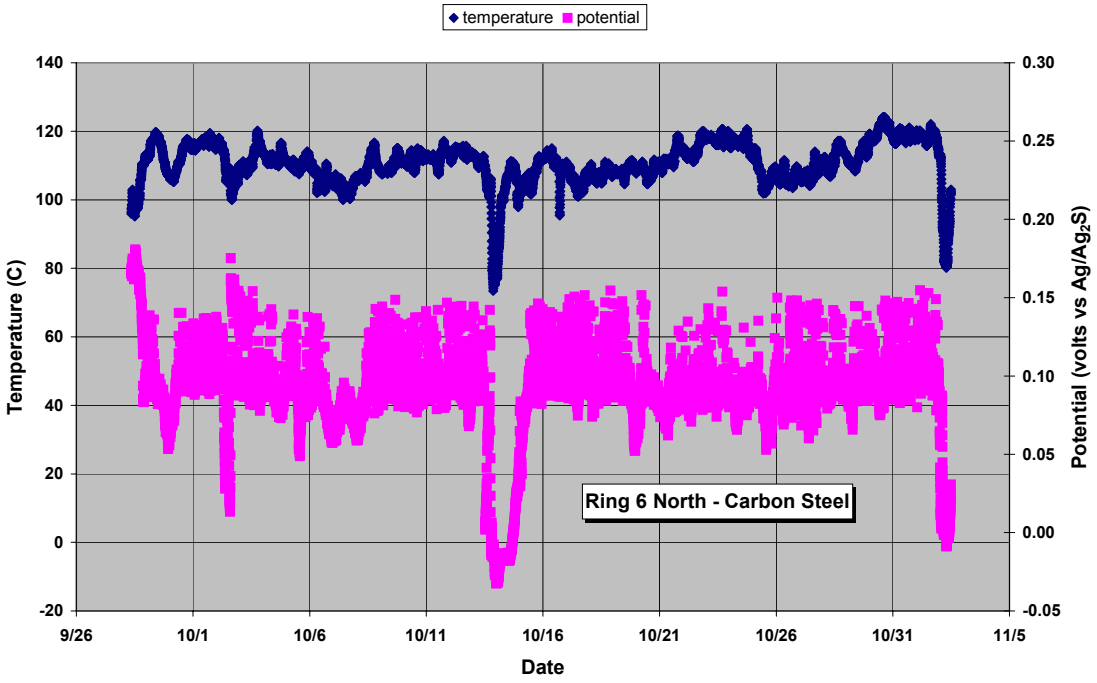

Fig. 52. Temperature and potential for the steel electrodes in the ring 6N probe for the same period as shown in Fig. 51.

with a temperature deviation within the digester (which occurred coincident with a general upset within the vessel). The other extended potential decrease – less dramatic and occurring on October 6-7 – has a slight average current increase associated with it, but no particularly sharp temperature change is associated with this potential behavior.

A subset of the time period shown in Figs. 51 and 52 is useful to compare the behavior and ECN characteristics of the steel electrodes in probes 6S and 6N. For example, a representative temperature comparison is shown in Fig. 53, and it shows that the temperature at ring 6S is routinely about 15°C higher than that at 6N. Note that the temperature indicated by each probe tends to exhibit changes that are qualitatively similar (magnitude, direction, and timing), but not precisely so. With only brief exceptions – one is indicated in Fig. 53 on September 28 – the temperature of ring 6S is always higher than that of 6N, yet the corrosion rate (calculated and observed) is considerably higher for the steel at 6N. Figure 54 gives the comparison of

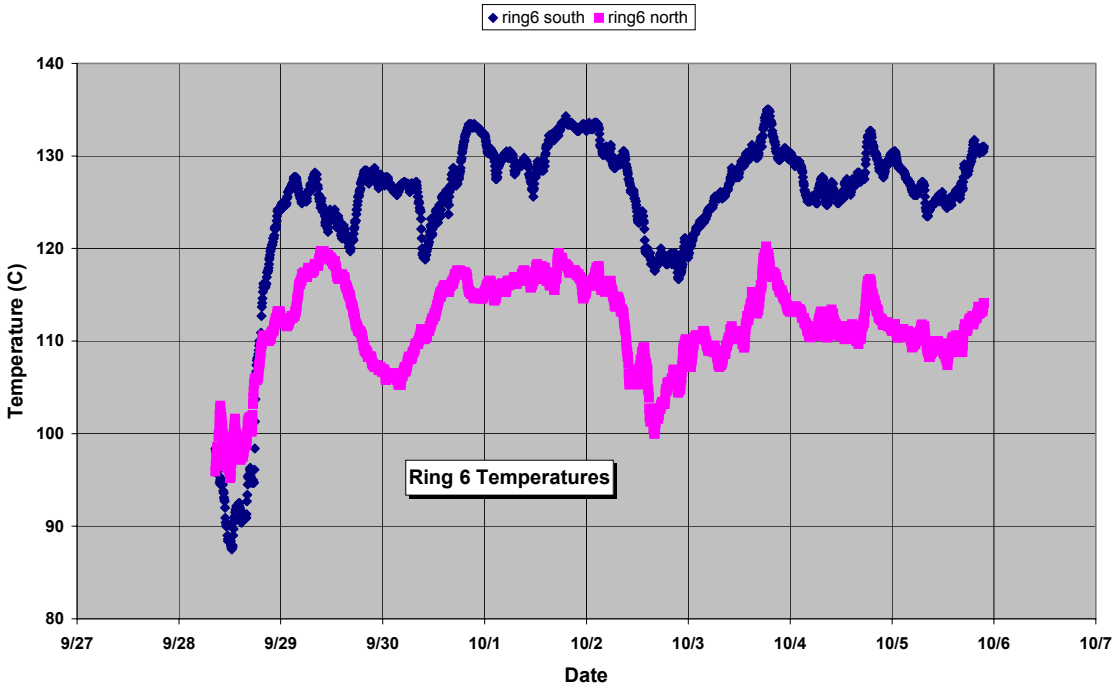

Fig. 53. Representative temperature comparison for the probes at positions 6N and 6S.

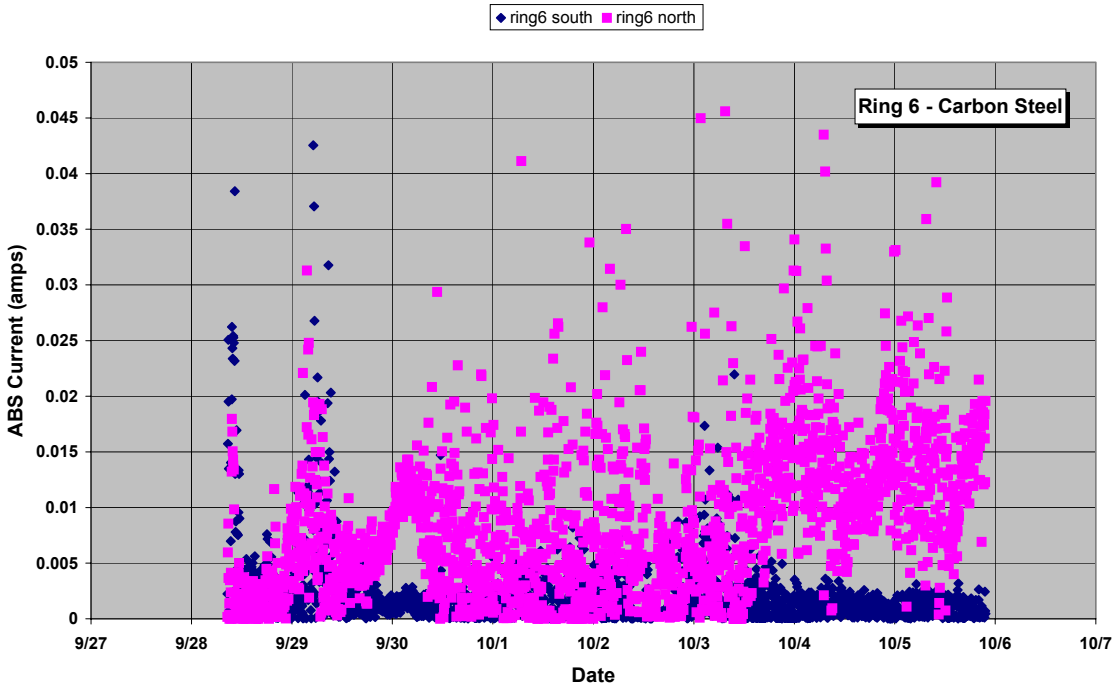

Fig. 54. Comparison of current noise (in absolute value) for the steel electrodes in probes 6S and 6N for the same period as that depicted in Fig. 53.

current activity in absolute value for these two probes for the same period as the temperature comparison on Fig. 53. The plot shows that the current associated with steel at ring 6S is routinely low with relatively little scatter compared to ring 6N. There are brief periods, however, in which the current activities are much closer to the same. Clearly, the ECN probes are detecting local changes in chemistry and wastage or redox conditions that cannot be tracked as operational variables by the mill.

The noise resistance parameter, R_n, is calculated by dividing the standard deviation of the potential signal (in volts) by the standard deviation of the current signal (in amps). Calculated this way, R_n has units of ohms and is inversely related to the corrosion rate through a multiplier called the Stern-Geary constant. In practice, the Stern-Geary constant is rarely known precisely but can be readily estimated for many situations. The noise resistance parameter was calculated continuously from the ECN data for each probe/material and it was found to be a poorly discriminating factor. Figure 55 shows the relative comparison of R_n for steel at Rings 6S and 6N for the same period as the current data shown in Figs. 53 and 54. Despite the fact that the ECN current magnitude is consistently greater for 6N by a factor of up to 7-8, the R_n data for steel at these locations is indistinguishable. Further, the variation of R_n with time is significant at each probe position, with changes of an order of magnitude common over a period of an hour or so, which is not similarly reflected in the current noise.

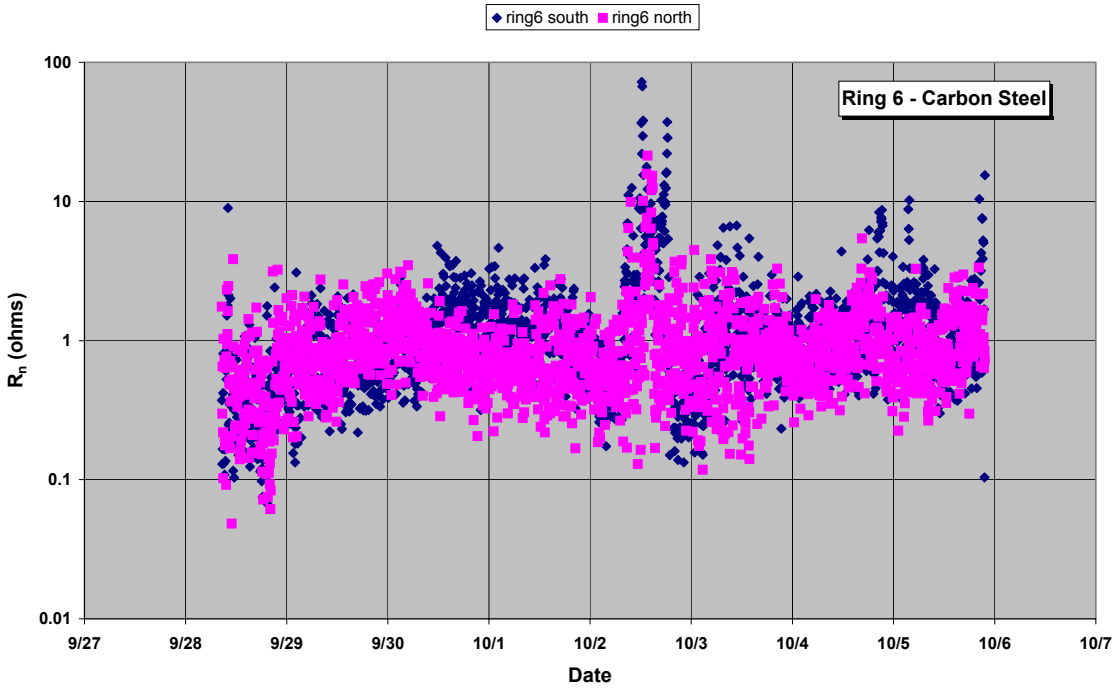

Fig. 55. Representative comparison of the noise resistance parameter for the steel electrodes in probes 6S and 6N.

Further, assuming a Stern-Geary constant of 22 mv [2], a corrosion rate on the order of 1000-10,000 mil/y is predicted for both steels from the R_n data in Fig. 55. Such a corrosion rate is clearly not consistent with post-test observation or corrosion current sums or with practical experience with steel in any continuous digester. In addition, the R_n values calculated for steel at rings 3 and 12 are not appreciably different from those at ring 6S and 6N. This result indicates the R_n data is perhaps influenced by redox reactions (which may be strongly temperature dependent), and in fact may largely reflect the resistance noise of the redox reactions rather than wastage reactions. Future work will examine possibilities for analysis in the frequency domain to separate wastage and redox reaction components to R_n.

The localization index (LI) is another calculated ECN parameter. LI is used to assess tendency toward localized corrosion and is calculated by dividing the standard deviation of the current signal (in amps) by the root mean square value of the current signal (also in amps). Calculated this way, LI is a dimensionless number between 0 and 1, with values toward 1 indicating increased localized corrosion (eg, pitting) tendency. Figure 56 shows – for the same time period as Fig. 55 – the calculated parameter LI for steel at rings 6S and 6N. Curiously, steel at rings 6S and 6N is predicted to suffer significant pitting tendency (LI at/near 1) for extended periods. Further, LI data for steel in the other probes also indicate significant tendency toward localized corrosion, particularly for ring 12, which shows an almost constant LI value of 1.0. In the post-test examination, only uniform corrosion was found on the steel electrodes at all locations, suggesting no merit for the LI parameter for steel in this environment.

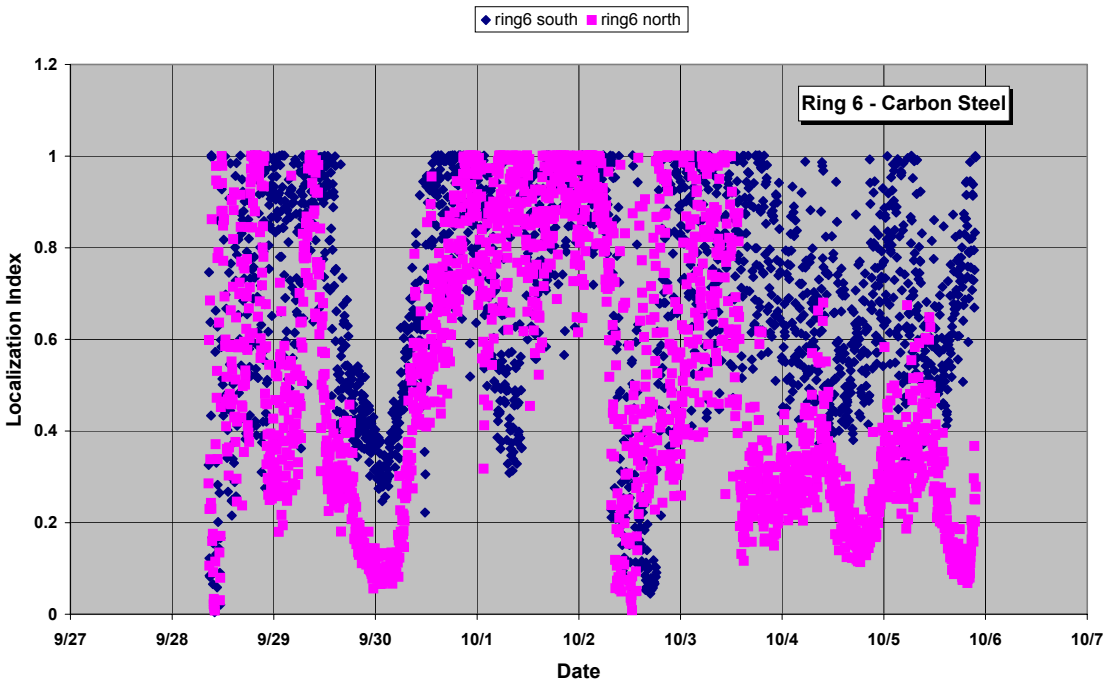

Fig. 56. Representative comparison of the localization index parameter for steel in probes 6S and 6N.

3.3.8 Carbon Steel Probes – Flash Tank

The flash tank probe was installed along with the digester probes in June 2001 but, due to limitations on the total number of channels in the instrumentation, data collection was not initiated until March 2002. [At that time, data collection from the probe at ring 12 was terminated.] Based on current sums prorated to the entire year of exposure, the corrosion of the steel in the flash tank probe was second in magnitude only to the steel at ring 6N. However, post test measurements and visual inspection indicated only modest corrosion of the steel electrode in the flash tank probe.

The ECN data for the flash tank steel revealed trends somewhat different than the steel in the digester. Figure 57 shows representative ECN data for the flash tank steel. Note that the plot of potential as a function of time indicates some "dual" character – the potential changes rapidly and nearly continually between about –35 mv (vs. Ag/Ag_2S) and something about 10-15 mv lower, giving rise to the potential curve that appears to have almost parallel components. The corresponding current activity is relatively high during the periods where the potential shifts back and forth between the two values and is relatively low when the potential simply remains at the slightly higher potential (e.g., April 7-8 and15-18). As shown in Fig. 58, the probe temperature does not seem to be a significant factor in the rapid fluctuation of potential. Since this behavior is also observed for the ECN data associated with the stainless steel probes, it seems likely that some feature of the flash tank environment is responsible. For example, the environment at the probe surface may tend to alternate between aqueous immersion and semi-liquid froth/foam created by the pressure drop of the hot liquid in the flash tank.

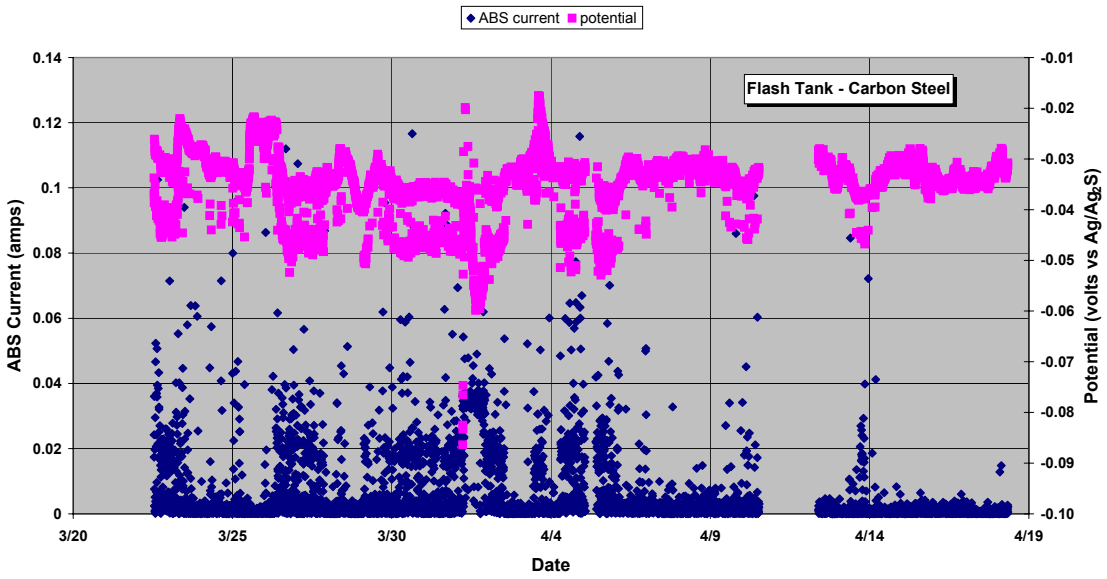

Fig. 57. Representative ECN data for the steel electrodes exposed in the flash tank. There is a gap in the data stream representing April 10-11.

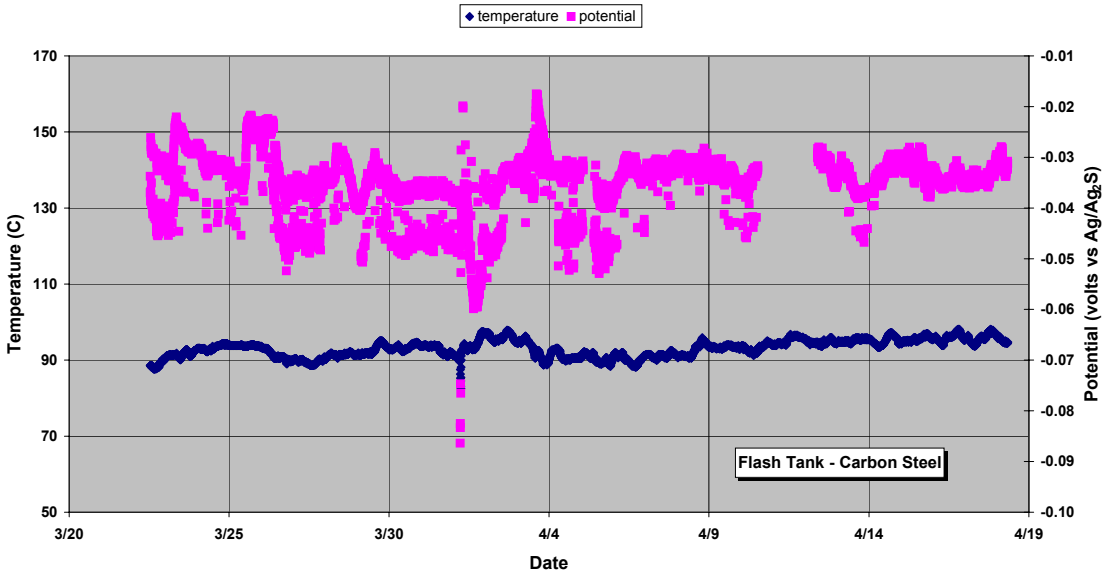

Fig. 58. Temperature and steel potential plotted together for the flash tank probe for the same period indicated in Fig. 57.

3.3.9 309LSi Stainless Steel Probes – Ring 12

The potential of the stainless steel electrodes at ring 12 varied only slightly over the entire duration of the experiment. With the exception of periods associated with start-up and shutdown or other significant vessel "upsets," the potential slowly drifted in the range –45 to –60 mv (vs. Ag/Ag_2S). The current activity was minuscule, but what little current activity was detected exhibited at least periodic bias from the beginning of the experiment. The bias was detected via a non-zero nominal current; that is, one of the pair of electrodes tended to become an anode for an extended period when, ideally, both electrodes should exhibit random anodic and cathodic behavior.

The noise resistance parameter (R_n), which was generally quite small, did not correlate well with the low current activity or the post-test observation indicating no corrosion attack. The localization index (LI) can best be described as "bipolar," meaning alternating intervals with a value of one or zero and very little else. Since the 309LSi electrodes were not attacked at all – much less exhibited any pitting or localized attack – this result indicates that R_n and LI are not applicable to analysis of the 309LSi corrosion in the digester at the position of ring 12.

3.3.10 309LSi Stainless Steel Probes – Ring 3

With the exception of wild fluctuations during start-up and shutdown, the potential of the 309LSi electrodes at Ring 3 changed from the range –40 to –60 mv early in the experiment to the range +10 to +70 mv (vs. Ag/Ag2S) later in the experiment. Although the potential did not change suddenly on any particular date, the potential exhibited quite a lot of scatter and fluctuation during January 2002 and, perhaps associated with the change to displacement washing in the same month, drifted to the latter potential value during this time, after which it remained more or less fixed in the higher range. The current activity was uniformly higher when the potential was in the higher range, but as previously indicated, none of the ECN current was associated with electrode wastage.

The values of R_n were not observed to change with the change in current activity and thus do not seem applicable to the analysis of corrosion at this location. The value of LI, however, was essentially zero throughout the exposure period.

3.3.11 309LSi Stainless Steel Probes – Ring 6S

Aside from the large variations noted for all probes during start-up and shutdown activities, the potential of the 309LSi at ring 6S showed three relatively distinct values. In the first few months of exposure, the potential slowly drifted in the range +20 to +60 mv (vs. Ag/Ag_2S). In January 2002, periodic shifts to the range 0 to –40 mv occurred, and finally, later in the year, the potential drifted to the range –20 to –80 mv. As observed for ring 3, the current activity for 309LSi at ring 6S decreased significantly at lower potentials but all of the current is presumed associated with redox activity. As for many of the 309LSi electrodes, the current data indicates significant bias (meaning electrode pair polarized such that there are semi-permanent anodes and cathodes rather than random fluctuations between electrodes) after a few months exposure.

R_n does not correlate routinely with current and not at all with corrosion rate. LI data indicates mostly general corrosion with brief periods of localized corrosion (which was not observed on the post-test electrodes).

3.3.12 309LSi Stainless Steel Probes – Ring 6N

The potential of the 309LSi electrodes at ring 6N varied only modestly over the entire duration of the experiment. Typically, the potential hovered in the range –30 to –45 mv or –45 to –60 mv (vs. Ag/Ag_2S) with gradual meanderings between these ranges. The current activity was relatively small throughout the exposure and the electrodes indicated at least periodic bias from early in the experiment.

R_n does not correlate with the low current activity or the absence of corrosion on the post-test specimens from ring 6N. LI data indicated extreme bipolar behavior despite the physical absence of corrosion of any type.

3.3.13 309LSi Stainless Steel Probes – Flash Tank

The average potential for the 309LSi in the flash tank drifted in the range of approximately –50 to –70 mv (vs. Ag/Ag_2S) over the entire data gathering period. Similar to the case for the carbon steel electrodes in the flash tank, however, the potential actually seems to exhibit rapid

and continuous fluctuations that are separated by about 10 mv. Figure 59 shows that, like the steel electrodes, the 309LSi current activity increases significantly during the relatively low potential periods and is near zero during the relatively high potential periods. While all of the current activity for the 309LSi showed bias, all of the largest current excursions seemed to occur on a specific electrode.

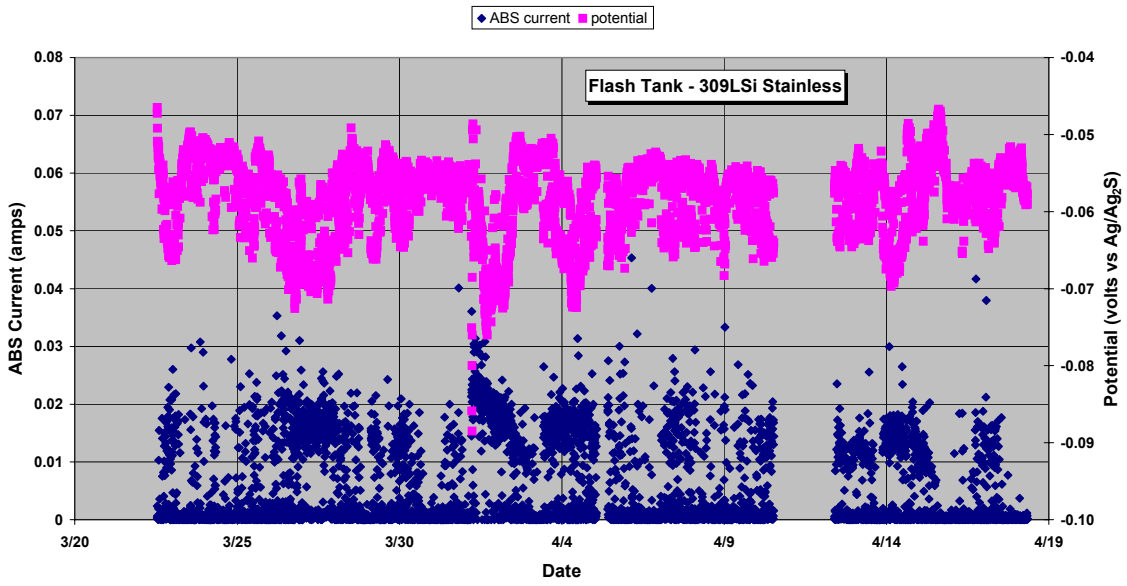

Fig. 59. Representative ECN data for the 309LSi electrodes in the flash tank. There is a gap in the data stream representing April 10-11.

R_n was not observed to correlate with current activity or physical observations. LI data exhibited values of near one almost continuously, suggesting localized corrosion that was not observed on the post-test specimens.

3.3.14 Effect of Temperature

As shown in a number of previous figures, minor variations in temperature do not appear to have a first order effect on potential and current activity for carbon steel or 309LSi in the digester environment. Occasionally, a significant temperature drop (> 10°C) – perhaps

associated with a brief upset in the vessel – corresponds directly to a change in potential, but there are many similarly sized potential changes that occur with no change in temperature. This result is consistent with results of ECN data for carbon steel collected at the Kamloops digester [1]. Further, significant changes in ECN activity for the carbon steel electrodes rarely coincide with changes occurring for the 309LSi stainless electrodes, even though temperature changes precisely the same for all electrodes on a given probe.

3.3.15 Effect of Other Process Variables

Variations in operational parameters were examined for correlations with changes in ECN behavior in two ways. Much of the analysis work was performed via visual examination of graphical representations of ECN data and process parameters plotted on the same time scale. In addition, detailed correlation coefficient analysis was performed.

The emphasis for the graphical effort was to identify particular values (or ranges) for specific process parameters that correlate significantly with changes in corrosion activity for at least one of the corrosion probes. This task was quite tedious but was simplified somewhat by the fact that, for weeks or months at a time, many of the operational parameters tracked by the mill exhibited very little change/scatter around a set-point determined by the process control requirements. Further, unlike a more unbiased mathematical/statistical approach, the graphical technique allows for human judgment/interpretation that can perhaps identify subtle trends in small subsets of the data that would be lost in the noise of the overall statistics. For example, the aggressive influence of Douglas fir on ECN characteristics of steel was not identified by correlation coefficient analysis in a similar experiment at Kamloops [1] but was detected graphically by examination of small subsets of data.

In summary, the graphical representations of process parameters and ECN data did not yield any reproducible correlations. One example of the process parameter data is shown in Fig. 60, which shows the "c" titration value of the white liquor feed to the digester. [The "c" titration in ml HCl x 3.1 gives the active alkali as g/l Na_2O.] The titration is nominally performed every 2-4 hours, so compared to ECN data that is measured every second and averaged on five minute intervals, this chemistry data is recorded/updated much less frequently. The alkali charge to the digester varies somewhat over long periods because it is

adjusted periodically to account for changes in white liquor strength and chip feed rate to the vessel. It is clear from Fig. 60 that the total scatter in the alkali charge remains only about ± 1.5% over long periods of time with predominantly gradual changes between extremes. The current sums and potential values, along with variations of each, were compared for each probe/material at the nominal value of alkali concentration (33.9%, indicated by horizontal dashed line, several different time periods) and compared with the equivalent values for the unusually low % alkali period (designated "low" on the graph, average value 32.4%) and the period of unusually high alkali (designated "high" on the graph, average value 35.0%). No consistent trends in current or potential – or any calculated ECN parameter – were detected as a function of the white liquor alkali concentration.

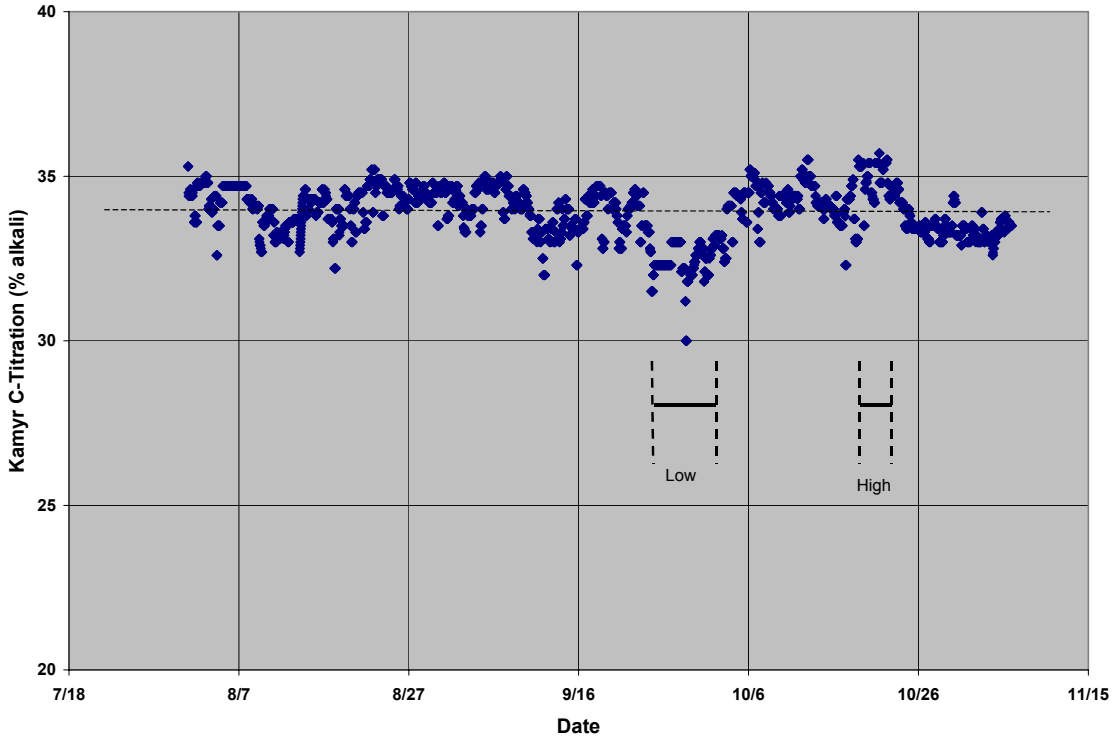

Fig. 60. Variation in the total alkali (%) calculated from the c-titration on the white liquor feed to the digester. The mathematical average for the period is given by the horizontal dotted line, and the periods with the largest deviation from the nominal value are noted as "high" and "low" on the graph.

Figure 61 shows a different type of change in a process variable as a function of time. The total filtrate flow rate for the period indicated is about 425 gpm, but there is a step-function change in the nominal value from relatively high (average of 488 gpm from January 20-25) to a low value (average of 366 gpm from January 25 – February 4) and returning to a high value (average of 459 gpm from February 4-11). Again, various ECN parameters during the indicated periods were compared as a function of total filtrate flow and no correlation could be identified.

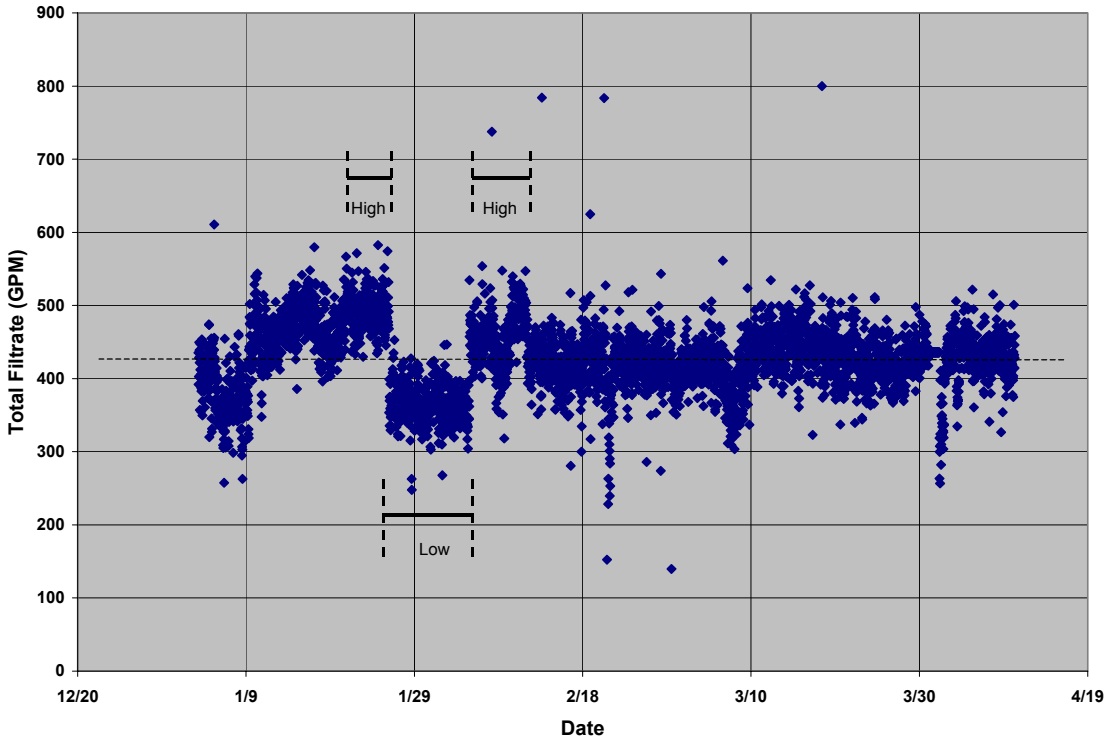

Fig. 61. Representative variation in the total filtrate flow rate as a function of time. The mathematical average value for the period is indicated by the horizontal dotted line, while periods of particularly high or low values are noted.

Another type of change in the process data that was examined is represented in Fig. 62. The operational parameter in this example is the current requirement for the outlet device, which is an indicator of production rate and a variety of chip/pulp mass properties. The

nominal value for the period shown is about 101 amps, but the scatter is routinely ± 10-15%. Late in the period depicted in Fig. 62, the current demand for the outlet device begins a sustained increase in the average value with the average increasing from about 100 amps (on April 3) to almost 120 amps (on April 26). Subsequently, a sustained but slow decrease to the nominal value occurs. Again, the ECN parameters do not reflect a consistent change in response to this (or any similar) change in digester operation.

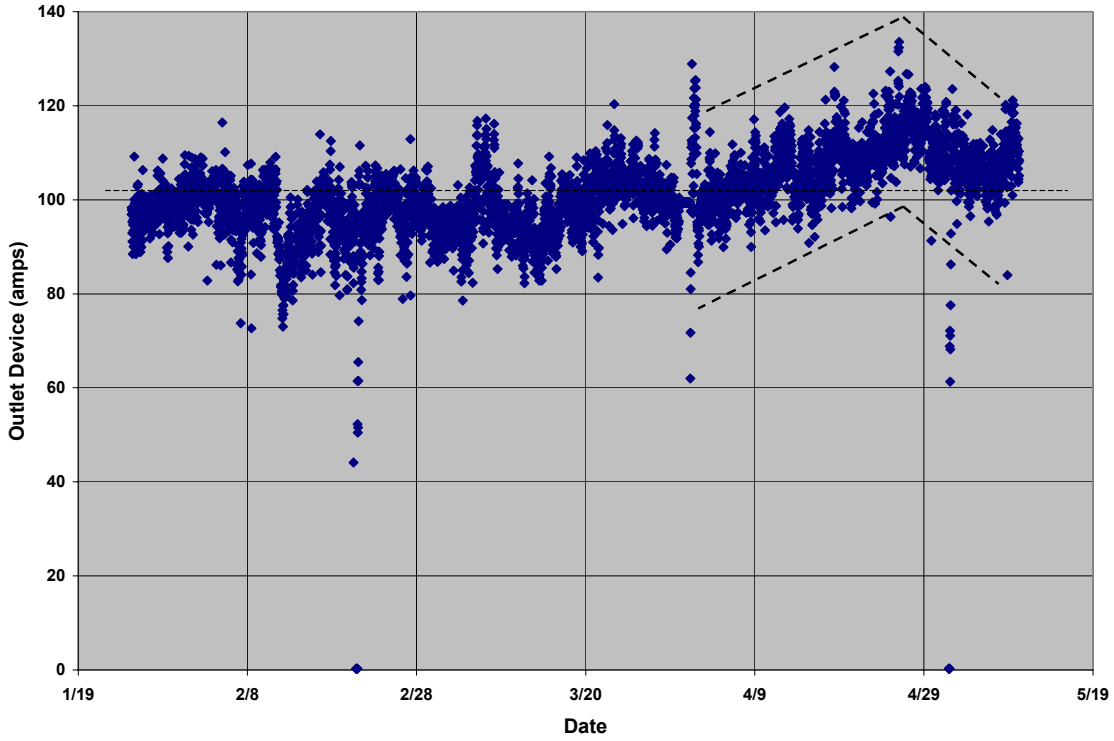

Fig. 62. Representative variation in the current demand by the outlet device as a function of time. The period marked by the sloped dotted lines indicates a sustained period in which the current demand increased followed by an extended period of decreasing demand.

For the correlation coefficient analysis, each process variable and ECN parameter – measured or calculated – was paired against every other available process/ECN parameter for each 24-h period of data collection over the course of the experiment. In addition to instantaneous correlations, delay times of up to two hours in 15-minute increments were included in the analysis. The rationale behind the delay times was to recognize that there is

potentially a time lag between a change in any particular process parameter and a response of any kind in the vessel. For example, for a delay time of 30 minutes, data for variable "x" were plotted against data for potentially dependent variable "y" collected 30 minutes from the corresponding time-tag value for "x."

From each pairing – with and without delay time – an correlation coefficient (R) for each day/combination was calculated. Values of +1 indicate direct linear correlation, values of –1 indicate direct negative correlation, and values of zero indicate no linear correlation. Similar to the result for the Kamloops experiment [1], no significant correlation was found between any measured/tracked process parameters and corrosion activity. Expressed mathematically, no average values of R greater than about 0.7 were observed at all, and no sustained values above about 0.4 were observed. This indicates that corrosion activity – based on ECN data – is not linearly related to any process parameter that is monitored at Spring Grove. Further, this result also suggests the process data is not related to itself via relationships that might be expected due to process control/logic. That is to say, none of the process variables correlated with any other process variables, which suggests that these factors are independent of each other rather than related through the control scheme.

There are many potential explanations for the apparent absence of correlations. Clearly, it is possible – even likely – that the process parameters used to control the process in order to generate a particular kappa number or some other key value have no particular bearing on the corrosion processes inside the vessel. For example, only limited chemistry data is collected and typically only on four-hour intervals. [In fact, a few of the chemistry variables were assessed only once or twice per 24-h period.] Perhaps the tight process control itself, which limits the frequency, magnitude, and duration of the changes in the recorded process parameters, also renders establishment of strong correlations difficult. Further, possible correlations among the recorded variables may be non-linear or multi-variable rather than linear relationships. Such a complex relationship would be very difficult to detect in such a large array of variables, particularly when there are no known outcomes on which to base a model.

Examination of the wall thickness and corrosion rate data (Figs. 2 and 3) indicates that some significant process change occurred on/about 1994 to adversely influence the steel corrosion rate. Coincident with that timing, the mill commenced operation of an oxygen

delignification system beginning in July 1994. It is not clear precisely how an oxygen delignification system would accelerate corrosion of steel in the vessel, most dramatically at a level just below the extraction screens. Certainly, the possibility of new/additional sulfur profiles and reaction products resulting from the process such as organic acids [4] could contribute to changes in steel corrosion as these components find their way into the digester system via the chemical (re)cycle that includes filtrate and brown stock wash, which is recirculated in limited quantities to the bottom portions of the digester. For example, increased thiosulfate concentration – generally considered aggressive toward carbon steel in alkaline digester environments – is a likely result of such a process. Lower cold blow filtrate residual alkali, which could occur as a result of oxygen delignification, is also a possible contributor to the increased corrosion rate in the lower portion of the digester.

In addition to rather poorly understood/defined chemistry changes, the digester operation was significantly perturbed by the introduction of the process. During initial implementation, there were very frequent starts/stops of the vessel – sometimes as many as five or six times a day for an extended period – while the system was brought on line. As start/stop transients have already been identified as relatively aggressive corrosion events, it is possible that the destruction of a protective passive film during the commissioning of the process contributed to the observed change in corrosion patterns. Since the details are poorly appreciated at this stage, further study on the effects of oxygen delignification on digester corrosion seems warranted.

Throughout the 1990s, other rather gradual changes have also occurred in the operation of the pulp mill. For example, the sulfidity of the process has slowly increased from 18-22% a few years ago to something in the range 24-28% currently. [Sulfidity of the liquor is defined as the ratio of Na_2S to active alkali (the sum of Na_2S and NaOH, both expressed as equivalents of Na_2O).] As a stand-alone variable, increased sulfidity is often associated with increased aggressiveness of pulping liquor towards carbon steel. However, the sulfidity did not change in step-function fashion at any point or even uniformly change (increase or decrease monotonically) for any specific period, and sulfidity does not change in isolation from other parameters in the process. Other changes that have occurred simultaneously through the early and mid-1990s include an increase in the non-process element concentration (notably chlorides) resulting from increased recycle and environmental regulations, and a change in management of the wood yard, which results in reduced residence time for chips on the pile

(which influences moisture content and chemistry). In addition, the lower cooking zone has been operated about 5° hotter over the past several years compared to previous set-points as the production rate has increased slightly.

Ultimately, corrosion monitoring during process changes such as these stands to shed more light than after-the-fact speculation. The ECN probes were in place for one recent process change – displacement washing was initiated in Jan 2002. Displacement washing involves reducing the amount of extraction liquor taken from the conventional extraction zone and moving the balance down to the wash zone. In addition, some of the wash recirculation is replaced with weak filtrate from post-digester washing. The intent of the change is to improve column movement, increase the residual alkali between the extraction zone and bottom of the digester, and cool the bottom of the digester a few degrees.

Immediately upon implementation of displacement washing, the ECN probes detected a significant decrease in current activity for the steel at ring 3 (most likely to be affected due to its position at the bottom of the digester). However, within about a month, corrosion activity for the steel at ring 3 had increased to levels slightly above the year-long average. Corrosion of steel at the ring 6 probes was unchanged or slightly decreased in the month following the change to displacement washing, but corrosion activity at both ring 6 steel locations increased significantly between February and the shutdown in May 2002. Redox activity for the stainless steel electrodes decreased significantly for several locations as a result of the change to displacement washing, but increased for stainless steel at ring 3. [Since no physical wastage was observed for the stainless steel electrodes, all current noise was assumed to be related to redox activity.]

3.3.16 Effect of Start-up and Shutdown

ECN data was collected for a portion of the initial start-up event, a significant portion of the shutdown/restart at the end of 2001, and several days into the final shutdown in June 2002. The probes experienced relatively violent changes in potential, current activity, and temperature during these transients. While it is true that the current sums do not seem to correlate very well with actual corrosion damage on the probes in this particular experiment, the potential swings (hundreds of mv) and current activity (orders of magnitude increase)

suggest that these transients are relatively aggressive corrosion events. In some cases, the potential and current tend to stabilize briefly at values significantly different from those occurring during operation, but this behavior could be correlated with the acid cleaning procedure.

Related to start-up and shutdown events, there are specific brief upsets in the vessel operation that typically involve the previously mentioned chip feed problems or 8-h maintenance efforts. These events require repressurization of the digester to bring the vessel back to full operation. During these restart conditions, internal flow, temperature, and chemistry conditions vary wildly (for a brief time) and are not indicative of steady-state operation. At high frequency, these events no doubt contribute significantly to accelerated corrosion of a steel vessel.

4.0 CONCLUSIONS

The initial ECN experiment in the digester at Spring Grove operated continuously for one year with only brief/minor interruptions in data gathering and no disruptions to the digester operation. The probes performed as intended with no failures of materials, equipment, or breaches of the pressure boundary.

The corrosion data derived from the ECN probes generated mixed results. The current summing technique to assess corrosion activity correctly identified the ring 6N steel with the highest general wastage rate – about twice that of the ring 6S steel. This trend was consistent with the historical observation that corrosion on the ring 6N side of the vessel was considerably larger that at the same elevation on the 6S side of the vessel over the last few years, but calculated wastage rates for both electrodes – using current sums – were lower than the actual measured values by a factor of 6-8. The steel at ring 3 also exhibited a significantly higher actual wastage compared with the current sum for the period, while current sums for the steel at ring 12 and in the flash tank corresponded very well with actual corrosion rates. The actual corrosion rates exhibited by all the steel electrodes in the digester were considerably higher than historical rates for corresponding probe positions in the vessel, suggesting that the recent trend of high corrosion rates on steel is accelerating. The 309LSi stainless steel overlay applied to the vessel shell on rings 5 and 6 just before this experiment performed exceptionally well, exhibiting no evidence of general wastage or pitting.

Consistent with the observed performance of the 309LSi overlay, none of the 309LSi stainless steel electrodes in the digester or flash tank revealed any evidence of corrosion. However, the current sums generated from the ECN data indicate variable degrees of corrosion activity. In particular, the stainless steel electrodes at ring 6S and ring 3 exhibit an order of magnitude greater current activity than their counterparts at ring 6N and ring 12. Significant ECN current activity in the absence of corrosion indicates that redox reactions rather than wastage reactions are dominating the noise measurements. All electrodes (stainless steel and carbon steel) exhibited noise resistance values much too low for the observed corrosion rates, again suggesting that the ECN calculation of noise resistance is dominated by the high frequency redox reactions in the Spring Grove digester. Future research should attempt to separate redox and wastage components of the ECN signals.

Attempts to correlate changes in ECN corrosion activity with changes in individual process parameters that are tracked by the mill were not successful. Aside from start-up and shutdown transients, including somewhat frequent "upsets" in the vessel in which most/all of the process parameters deviate significantly from nominal set points for a brief period, no individual process parameters correlated significantly with ECN activity. These operational transients are aggressive corrosion events but, fortunately, are relatively short-lived in the scope of overall service duty. Further, no individual process change such as the introduction of oxygen delignification could be associated in a specific way with accelerated corrosion of the steel vessel. Attempts to find such correlations are complicated by the fact that process parameters rarely change in isolation from other variables, and that many of the variables that are tracked are for the purpose of generating product with particular properties as opposed to understanding corrosion in the vessel.

ACKNOWLEDGEMENTS

This research was funded by the United States Department of Energy Office of Industrial Technologies for the Agenda 2020 Program. The Oak Ridge National Laboratory Program Manager for this effort was P. Angelini. The industrial advisory board consisted of M. E. Gorog (Weyerhaeuser), W. B. A. Sharp and S. J. Lukezich (MeadWestvaco), and D. C. Crowe (International Paper). The entire staff at Glatfelter in Spring Grove was helpful and made probe installation and data transfers seamless – in particular, D. E. Roy, H. E. Muller, R. C. Abel, and G. L. Wisner facilitated information exchange and technical support and were very available to ORNL. In addition, B. Keeney (formerly of Glatfelter) and T. Redding (Glatfelter) were instrumental in providing computer access to the digester process data. S. J. Lukezich (MeadWestvaco) provided material for fabrication of the 309LSi electrodes. E. T. Manneschmidt and K. A. Choudhury provided computer graphics/image file support and H. F. Longmire provided metallography support. J. R. Keiser (ORNL) provided technical support and, along with P. F. Tortorelli (ORNL), reviewed the manuscript.

This page
intentionally blank

REFERENCES

1. S. J. Pawel, D. W. Townley, M. E. Gorog, and D. F. Wilson, "Correlation of Process Data and Electrochemical Noise to Assess Kraft Digester Corrosion: Kamloops Experiment," Oak Ridge National Laboratory Report **ORNL/TM-2002-33**, April 2002.

2. J. J. Perdomo, P. M. Singh, P. R. Conde, and S. J. Pawel, "Applicability of Electrochemical Noise Measurements in Kraft Pulping Liquors," submitted to *Corrosion Journal.*

3. D. W. Townley, S. J. Pawel, D. F. Wilson, and D. E. Roy, "Investigation of the Use of Electrochemical Noise to Monitor Corrosion in Kraft Pulp Digesters," **CORROSION'03** (NACE) paper #3411.

4. C. W. Dence and D. W. Reeve, eds., **Pulp Bleaching: Principles and Practice**, Tappi Press, Atlanta, GA (1996) 215-239.

This page
intentionally blank

APPENDIX A – Corrosion Rate Calculation from Current Sums

The fundamental relationship of interest is Faraday's Law, expressed as the definition of current, is:

$$I = [\ W / M \cdot t\ ]\ N_o \cdot m \cdot e^+ \qquad (1)$$

where I is current (coulombs/sec, or amps),
W is mass in grams (of Fe, in this case) dissolving as a result of corrosion in time t,
M is the atomic weight of the corroding material (g/mol),
t is the cumulative time of corrosion (seconds) ,
N_o is Avagadro's number (6.023×10^{23}/mol),
m is the oxidation state on the corroding ion, and
e^+ is the unit charge of electricity (1.60×10^{-19} coul).

Equation (1) can be manipulated to a more useful form as:

$$W \text{ (in measurement time t)} = [\ I \cdot t\ ] \cdot M / [N_o \cdot m \cdot e^+]. \qquad (2)$$

Expressed this way, the quantity [I · t] is the number of coulombs Q that is the integrated area under the amps vs. time curve that the ECN data produces.

Since it can be assumed that the primary corrosion reaction of steel in the digester liquor is

$$Fe \rightarrow Fe^{2+} + 2e^-$$

"m" in Equation (2) is 2. Of course, further oxidation to the Fe^{3+} can also occur, but this is not typically the initial reaction and the one detected by the probes.

Therefore, substituting appropriate numbers into Equation (2):

$$W \text{ (in measurement time t)} = Q \cdot (55.85 \text{ g/m}) / (6.023 \times 10^{23} \text{ /m}) \cdot (2) \cdot (1.60 \times 10^{-19} \text{ coul})$$

which reduces to

$$W \text{ (g, in measurement time t)} = Q \cdot (2.90 \times 10^{-4}). \qquad (3)$$

To convert the mass loss (W) to a penetration (P), it is necessary to assume that the mass loss is uniform over the exposed electrode area (which was confirmed by post-test inspection of the electrodes for all probes). If the corrosion is uniform, the mass loss can be converted to a penetration by dividing by the density of the material (Fe = 7.86 g/cm^3) and the exposed electrode area (sum is 1.24 cm^2 for the pair of electrodes in each probe). Substituting into Equation (3):

$$P \text{ (cm, in measurement time t)} = Q \cdot (2.90 \times 10^{-4}) / [(7.86 \text{ g/ cm}^3) \cdot (1.24 \text{ cm}^2)]$$

and

$$P \text{ (cm, in measurement time t)} = Q \cdot (2.98 \times 10^{-5}). \qquad (4)$$

To modify Equation (4) to the more useful units of mm or mils, the conversions are

$$P \text{ (mm, in measurement time t)} = Q \cdot (2.98 \times 10^{-4})$$

or

$$P \text{ (mils, in measurement time t)} = Q \cdot (1.17 \times 10^{-2}).$$

Therefore, for any total measurement time t, the current sum Q over that period may be used to calculate the penetration rate consistent with the previous assumptions. As an example, consider a 100-day period (0.274 years) over which a probe passed a total of 254.1 coulombs. The corresponding penetration rate is then

$$\text{Penetration rate (in mils/y)} = (254.1) \cdot (1.17 \times 10^{-2}) / (0.274 \text{ y}) = 10.8 \text{ mils/y}.$$

Of course, the rate so calculated is only an estimation, because the current detected by the ZRA is only net current – some of the corrosion current self-terminates on each electrode (does not pass through the ZRA). In addition, redox reactions on the electrode surfaces possibly contribute to current detected by the ZRA, although in the general sense this contribution should approximate white noise for each electrode in a probe and cancel out as zero net contribution.

APPENDIX B – Process Data Collected at Spring Grove

The list below represents the operational and process data information provided to the project by Glatfelter personnel. The function/purpose of each of these process parameters is beyond the scope of this documentation, but these are the digester-oriented parameters tracked by the mill operators to control the process. These data, recorded on various intervals from continuously to once or twice per day, were used in an attempt to find correlations between one or more of these and corrosion activity as defined by the ECN probes.

digester pressure (psig)
steaming pressure (psig)
kamyr % active alkali on wood
digester level
permanganate number – upper
top separator (amps)
outlet device (amps)
black liquor residual alkali (g/l as Na_2O)
quench dp (psi)
extraction dp (psi)
kamyr c-titration (% alkali)
total filtrate (gpm)
wash circulation (gpm)
extraction flow (gpm)
blow flow – spare (gpm)
blow flow – normal (gpm)
lower cooking circulation (gpm)
upper cooking circulation (gpm)
white liquor flow (gpm)
cold blow filtrate temperature
wash temperature
extraction temperature
blow line temperature – spare
blow line temperature
lower heater output temperature
lower heater inlet temperature
upper heater outlet temperature
upper heater inlet temperature
top circulation temperature
heater discharge temperature
Kamyr pre-O_2 permanganate number

This page
intentionally blank

INTERNAL DISTRIBUTION

1. P. Angelini
2. E. E. Bloom
3. G. E. Giles
4. L. L. Horton
5. J. R. Keiser
6-15. S. J. Pawel (10)
16. P. F. Tortorelli
17-18. D. F. Wilson (2)
19-20. Central Research Library (2)
21. Document Reference Section
22. ORNL Laboratory Records - RC
23. Office of Scientific & Technical Information

EXTERNAL DISTRIBUTION

24. D. C. Crowe – International Paper, Mfg. Tech. Center, 6285 Tri-Ridge Blvd., P.O. Box 7910, Loveland, OH 45140

25. M. E. Gorog – WTC1B40, Weyerhaeuser P.O. Box 9777, Federal Way, WA 98063-9777

26. S. J. Lukezich – MeadWestvaco Research Laboratory, 232 Eighth St., P. O. Box 1700, Chillicothe, OH 45601-5700

27-28. D. E. Roy – Glatfelter Company, 228 South Main St., Spring Grove, PA 17362

29. M. Salcudean – 1938 Western Parkway, Vancouver, V6T 1V5, British Columbia, Canada

30. D. Salem – DOE, Office of Industrial Technologies, EE-20, 1000 Independence Ave. SW, Washington, DC 20585-0121

31. W. B. A. Sharp – MeadWestvaco, Laurel Technical Center, 11101 Johns Hopkins Rd., Laurel, MD 20723-6006

32. D. A. Singbeil – Paprican, Vancouver Laboratory, 3800 Wesbrook Mall, Vancouver, British Columbia V6S 2L9, Canada

33. P. M. Singh – Institute of Paper Science and Technology, 500 10th Street, Atlanta, GA30318-5794

34-35. D. W. Townley – M. J. Schiff and Associates, 431 W. Baseline Rd., Claremont, CA 91911

36. D. A. Wensley – D. A. Wensley Consulting Engineering Services, 15397 Columbia Ave., White Rock, British Columbia V4B 1K1, Canada